I.O.S.

SOME CHARACTERISTICS OF ELECTROMAGNETIC CURRENT SENSORS IN LAMINAR FLOW CONDITIONS

by

G. GRIFFITHS, P.G. COLLAR AND A.C. BRAITHWAITE

Report No 56

1978

NATURAL ENVIRONMENT RESEARCH COUNCIL

INSTITUTE OF OCEANOGRAPHIC SCIENCES

INSTITUTE OF OCEANOGRAPHIC SCIENCES

Wormley, Godalming,
Surrey, GU8 5UB.
(0428 - 79 - 4141)

(Director: Dr. A.S. Laughton)

Bidston Observatory,
Birkenhead,
Merseyside, L43 7RA.
(051 - 653 - 8633)

(Assistant Director: Dr. D.E. Cartwright)

Crossway,
Taunton,
Somerset, TA1 2DW.
(0823 - 86211)

(Assistant Director: M.J. Tucker

INSTITUTE OF OCEANOGRAPHIC SCIENCES

SOME CHARACTERISTICS OF ELECTROMAGNETIC CURRENT SENSORS IN LAMINAR FLOW CONDITIONS

G. GRIFFITHS, P.G. COLLAR and A.C. BRAITHWAITE

REPORT NO. 56

1978

This work, and that in the accompanying report, No. 68, was supported by the Departments of Industry and Energy.

Institute of Oceanographic Sciences,
Wormley, Godalming, Surrey GU8 5UB.

CONTENTS

1. INTRODUCTION

The electromagnetic current meter is based on the principle established by Faraday, namely that the interaction between a magnetic field, $\underset{\sim}{B}$, and a conductor moving at velocity, $\underset{\sim}{V}$, produces an electric potential distribution in the conductor. If the moving conductor is a fluid in which displacement current may be neglected, Maxwell's equations show (Shercliff, 1962) that the potential distribution ϕ is given by: $\nabla^2\phi = \nabla.(\underset{\sim}{V} \times \underset{\sim}{B})$ and is independent of the electrical conductivity of the fluid. This equation may be solved provided the boundary conditions are known. In an ideal situation in which flow is laminar and uniform the potential difference between two electrodes normal to $\underset{\sim}{B}$ and $\underset{\sim}{V}$ is $\Delta\phi = LBV_{res}$ where L is the electrode separation and V_{res} is the component of velocity, $\underset{\sim}{V}$, resolved in a direction normal to electrodes and field.

These conditions do not obtain in a practical sensor head, which contains the magnetic field coils and sensing electrodes. The most serious limitations arise from modification of the flow by the head itself, and it is this aspect with which this report is mainly concerned. The design of the current meter drive and voltage potential sampling circuits is not considered. Details of the methods employed are given in Tucker et al. (1970) and Kanwisher and Lawson (1975).

Three types of sensor head, listed below and shown in Fig. 1, have been tested for response in laminar flow: a subsequent report will discuss their performance in turbulent flow.

(a) Discus head

This type of head was first developed by IOS for use as a ship's log (Tucker et al., 1970) and has since been used for two component current measurement in a number of applications.

(b) Annular head

In view of the limited directional response of the discus head, and the existence in many applications of flow components in three dimensions, an annular head is being developed at IOS. The magnetic field coil is of ellipsoidal cross section to minimize disturbance when flow is mainly in the plane of the coil. Four electrodes are mounted within the annulus, and provide potential differences proportional to two orthogonal components of flow resolved in this plane.

(c) Spherical head

This form has been developed in the USA (McBirney, 1975) and aspects of the performance in towing tank tests have been described by McBirney (1976) and Cushing (1976). The work described here has been carried out on a sensor head designed and constructed at IOS. The electrodes in this configuration are mounted at 90^{o} intervals in the equatorial plane. In view of the effects of flow separation on performance, measurements have been made with electrodes projecting 1.5 mm and 10 mm from the sphere.

A sectional view of each of the three types of head is given in Fig. 2. The discus head was a commercially manufactured item (Colnbrook Instrument Development Limited*, under licence to IOS); similar techniques were used in the construction of the experimental sphere and toroid. The results described below are in no way dependent on standards of manufacture. The measurements were made on individual heads over a period of several months; and each head was driven by the same electronics unit. Table 1 summarises the head characteristics.

2. EXPERIMENTAL DETAILS

A block schematic of the measurement system is shown in Fig. 3. Each sensor head was driven by the IOS Mk 3 electronics unit, which supplies a stabilized head current reversed at a 28 Hz rate to minimize electrode polarisation effects, and produces voltage analogues of the resolved flow components. The unit has good stability, and provides a well defined gain with high rejection of common mode signals. A low pass filter is included, with a cut-off at 5 Hz. Additionally, an external amplifier with a switched gain from 1 to 5, and a second order low pass filter with a cut off at 3 Hz was used. The two outputs from the filters (x and y axes) were displayed on a storage oscilloscope, an ultraviolet chart recorder, and a digital voltmeter, with a resolution of 0.1mV. The oscilloscope and the voltmeter were used to indicate any residual currents in the tank after each experiment, dye was also used to detect any disturbance in the water. The current meter outputs were also taken to a data logger, with a single sample resolution of 17mV (about 6 mm/sec^{-1}). Where possible an attempt was made to log at least 200 samples for each run. The sampling frequency of the data logger was 9.77 Hz, and this meant a maximum input bandwidth of 4.9 Hz.

*Colnbrook Instrument Development Ltd.,
Poyle Road, Colnbrook,
Bucks, SL3 0AJ.

The filters were considered adequate to avoid aliasing errors. The linearity of the data logger, filters and amplifier was better than 0.1%.

The measurements were made in the towing tank at IOS. This is of dimensions 50 × 2 × 2 metres and is filled with fresh water. It is equipped with a hydraulically driven carriage, whose speed can be preset within the range 1 cm/sec-2 m/sec. Except at the lowest part of the range, speed is constant to within 1%.

Carriage speed is available as a variable pulse frequency analogue, obtained by interrupting a light source-detector path with a slotted wheel, geared to a ground steel wheel spring loaded on the running rail. The logger counts these pulses continuously and samples the counter synchronously with other channels.

We have also attempted to simulate near-surface dynamic conditions by mounting on the tow carriage an apparatus which moves the instrument in a vertical, circular path of adjustable diameter 25-100 cm and periodicity within the range 5-33 seconds (Fig. 4). This is driven by a servo-controlled motor which generally assures constancy of angular velocity to within 2%. The device also carries a shaft encoder to permit correlation of current meter output with flow incidence angle.

Measurements were made of sensor linearity, response to flow in the plane of the electrodes (azimuth response), tilt response, and dynamic response. In addition comparisons were made of the fluctuations present in the outputs in steady flow conditions (hereafter referred to as noise). For two types of head (discus and annulus) the zero stability was checked in still water.

3. LINEARITY

Measurements of the linearity of the sensors were made between 2 cm/sec and 150 cm/sec with the electrode axes aligned along and across the tank. The lower speed limit was set by residual currents in the towing tank. Maximum errors due to these were estimated as ±2 mm/sec, in addition to the error deduced from the standard deviation of the sample population. The high speed limit was set by the onset of strumming of the support spar and the need for an adequate number of samples in the time available after acceleration and before deceleration of the towing carriage.

An unweighted linear regression has been applied to the data. Rather than plot the observations for each head against carriage speed we have plotted the residuals from the regression line (Figs. 5(c), 7(c), 9(c))

which show more clearly deviations from linearity. Sensitivity, defined as $\frac{\text{current meter output}}{\text{carriage speed}}$ is plotted in Figs. 5(a), 7(a), 9(a). This, also, reveals any non-linearities in the output, although it requires an accurate measurement of output in zero flow so as to avoid distortion of the calculated sensitivity at low speeds.

Fluctuations occurred in sensor output at all speeds (hereafter referred to as 'noise'), increasing generally with increasing speed, as shown in Figs. 5(b), 7(b), 9(b), in which standard deviation from the mean is plotted against speed. In order to indicate the degree of uncertainty this has introduced into mean values, a normal distribution has been assumed and 95% confidence limits have been calculated for each point in the sensor response.

(a) Annulus

Figs. 5, 7 and 9 show that the performance varies appreciably between the different head types. The best linearity is obtained with the annular head. The residuals plotted in Fig. 5(c) do show systematic departures from linearity, but these are small, $\sim$2 mm/s at 1 m/s. Note that the reduction in sensitivity shown in Fig. 5(a) below about 15 cm/s was not reproducible: on reversing the tow direction, the sensitivity was found to increase at low speed. These changes are thought to result from residual currents in the towing tank (typically $\lesssim$2 mm/s) and are not attributable to the sensor itself. The good linearity can be attributed to the absence of boundary layer and flow separation effects near the electrodes. The presence of a boundary layer near the electrodes can significantly affect performance, as in the case of the spherical or discus heads - discussed below.

For the annular head, we may use expressions derived by Shercliff, 1962, for the sensitivity of a coil situated behind an insulating wall, since the potential distribution can be shown to be symmetrical about the plane of the ring.

Thus sensitivity $S \sim \frac{0.2\pi Nil}{d}$ μV/m/s

where d = coil diameter N = number of turns

l = electrode spacing i = coil drive current

We thus expect annular coils I and II (Table I) to have sensitivities $\sim$80 and 17 μV/m/sec respectively. Measured values were 87 μV/m/s and 22 μV/m/s.

Table I

Principal characteristics of e.m. sensor heads

Annulus	I	II
Coil:	530 turns	230
	15 cm mean dia.	15 cm
	40Ω resistance	24Ω
	0.4 amp current	0.2 amp
Electrode separation:	10 cm	10 cm
Sensitivity:	87 μV/m/s	22 μV/m/s

Version II was identical in exterior dimensions to I.

All tests described in this report were made on I.

Discus

Coil:	380 turns
	8 cm outer dia.
	18Ω resistance
	0.4 amp current
Electrode separation:	8 cm
Sensitivity:	102 μV/m/s

Sphere

Coil:	760 turns
	8 cm outer dia.
	36Ω resistance
	0.4 amp current
Electrode separation:	15.4 cm 13.7 cm
Sensitivity:	~65 μV/m/s

See Fig. 14 for the effect of electrode protrusion on sensitivity.

Contributions to the noise in perfectly laminar flow can arise from five main sources:

(a) Disturbance to flow induced by the physical presence of the sensor head.

(b) Vibration of the sensor due to fluctuations in carriage motion. This can interact with the effects of (a).

(c) Stray electromagnetic potentials appearing at the electrodes. These can make measurements difficult in fresh water filled towing tanks, although no such difficulty has been experienced in the present measurements. In seawater the source resistance is a factor $\sim$40 lower, and the external electrical noise generally negligible.

(d) Electronic noise arising mainly in the first stage of the current meter electronics. At 300^{o}K thermal noise at the sensor head is $\sim(1.65.10^{-20}.RB)^{\frac{1}{2}}$ where R is the source resistance ($\sim$3kΩ for the annular head), and B is the bandwidth. Allowing for noise bands at harmonics of the field reversal frequency a value ~30 Hz may be assigned to B. Given a sensitivity of $\sim$80 μV/m/sec an r.m.s. noise level of $\sim$0.05 cm/s is obtained.

(e) Quantisation noise arising from discrete sampling of the current meter signal. Irish and Levine (1978) have shown that, for a system in which a frequency analogue of the signal is sampled, r.m.s. noise is $\sim c/\sqrt{6}$ where c is the least count. For most annular head measurements quantisation noise was $\sim$0.21 cm/sec.

At very low speeds (Fig. 5b), noise levels are generally comparable with quantisation levels, although the reason for slightly lower values at around 10 cm/s is unknown. Thus experiments to determine low speed responses would require a much lower quantisation threshold. At higher speeds the noise levels for the longitudinal axis are generally similar to those arising from carriage speed fluctuations: exact comparison is not possible since carriage speed fluctuations were not filtered as heavily as the current sensor outputs.

The spectral distribution of the longitudinal axis noise at 20 cm/s is shown in Fig. 6. In this measurement a lower quantisation interval was used. Note that most energy lies below 1 Hz. The total variance for the measurement was 0.0144 $(cm/s)^2$. This is somewhat greater than the estimate of thermal noise in (d) above; it is therefore unlikely that thermal noise predominates in these circumstances.

The transverse axis noise levels are considerably greater than for the longitudinal component, and these are almost certainly associated with the disturbance of the flow by the sensor itself. Unlike the case of thermal noise, a signal to noise ratio determined by hydrodynamic noise at a given point in the spectrum cannot be improved by increasing the coil drive power.

(b) Discus

In the case of the discus head an increase in sensitivity was obtained with increasing speed, although no observation lay more than 0.5 cm/s from the best linear fit. This departure from linearity is clearly not attributable to the effect of residual currents on low speed measurements. Studies were made at low speeds (<50 cm/s) of the flow around a discus head, using a potassium permanganate dye ejected through a fine orifice close to the forward stagnation point. These showed the flow to be attached to the face containing the electrodes throughout the speed range: some representative photographs are shown in Fig. 8. The region of reverse flow, and formation of a vortex to the rear of the separation point, is clearly visible. Changes in the boundary layer thickness with speed may be responsible for the change in sensitivity. Appendix 1 examines the likely order of the effect.

The noise levels recorded for the discus head were consistently lower than for either of the other two sensor types. Note that the current sensor noise is partly correlated with carriage speed variance but is of lower magnitude, due probably to differences in filtering. Also the transverse axis has the least variance associated with it, and this is independent of speed. A similar thermal noise power to that for the annular head was obtained; this represented a slightly lower r.m.s. speed ($\sim$0.045 cm/s) due to the greater sensitivity of the discus head ($\sim$100 μV/m/s). The quantisation interval for these measurements was 2.07 mm/s, giving an r.m.s. quantisation noise level of 0.08 cm/sec. We conclude that for the discus head hydrodynamic noise is insignificant. The noise associated with the longitudinal axis is caused mainly by fluctuations in carriage speed, while for the transverse axis a combination of thermal noise and, in the present measurements, quantisation noise are the limiting factors.

(c) Sphere

Within the range of Reynolds numbers with which we are concerned $10^3 \lesssim R \lesssim 10^6$ there are two flow regimes. For $R < 1.5.10^5$ a laminar

boundary layer is present from the forward stagnation point to a subtended angle $\theta \simeq 83^{o}$. Flow separation takes place at this point: behind this is a region of reverse flow close to the surface.

For $R > 5.10^{5}$ the boundary layer becomes turbulent and separation is delayed until larger angles of θ have been attained. The value of Reynolds number at which transition occurs from a laminar to a turbulent boundary layer can be reduced by surface roughness or free stream turbulence. The importance of the boundary layer, and the magnetic field distribution within it, in determining sensitivity has been demonstrated by Cushing (1976) who has modelled the flow around a sphere in terms of a thin vortex shell (the boundary layer) outside which potential flow (zero viscosity) is assumed to exist. The further assumption is made that the boundary layer thickness increases as θ^{2}. For flow coplanar with the electrodes the analysis results in an expression for the sensitivity of the form:

$$S = (1 + \Delta S)(\cos\theta + \Delta c)$$

where ΔS defines the change in sensitivity with Reynolds Number at zero horizontal azimuth, and Δc is the deviation from perfect azimuth response at constant speed.

$$\Delta S = C_B R^{-\frac{1}{2}} A$$

and $\Delta C = (C_B R^{-\frac{1}{2}} B/(1 + \Delta S))\theta^{2}\cos\theta.$

A,B - 1.5, 3.5
determined empirically for
$R > 4.10^{5}$

The boundary layer coefficient C_B is determined by the gradient of magnetic field through the boundary layer and the relative electrode positions.

We have made several comparisons between the predictions of this analysis and our experimental results; also with data published for the Marsh McBirney 4" dia. spherical sensor. The theory predicts some of the trends, but we do not find good detailed agreement with observations. The reasons for this may include the facts that the flow conditions are more complex than the model describes, particularly beyond the flow separation point: also that the magnetic field distribution external to our sensor is not dipole-like.

Two versions of the IOS sphere were tested. In the first the electrodes projected 1.15 mm from the surface: in the second the electrodes were mounted 1 cm from the sphere. The results are plotted in Fig. 9. Of the three types of sensor head the sphere had the least linearity of output and greatest noise levels. The maximum departure from linearity in the speed range 0-150 cm/sec was ~5 cm/s for the sphere (Fig. 9c) compared

with 0.5 cm/s for the annular and discus heads. The sensor with 0.15 cm electrode protrusion exhibited the largest noise levels. Below 80 cm/s the noise generally increased steadily with speed although the transverse axis noise was again higher than the longitudinal component. At speeds below about 20 cm/s quantisation noise predominated, but above this there is little doubt that the noise was of hydrodynamic origin. Above 80 cm/s the behaviour became uncertain. Changes in output corresponding to 6 cm/sec amplitude and several seconds period were observed. Examination of subsets of the sample population at each speed in this region showed the statistics to be non-stationary and estimates of noise level and mean output are therefore less reliable. Normal distributions were again obtained at speeds above about 110 cm/s.*

The positioning of the electrodes further into the flow away from the boundary layer reduced noise levels markedly and improved linearity slightly. Little change was observed in sensitivity.

Fig. 10 shows, as a function of Reynolds Number, sensitivities deduced from measurements made by NOIC on a Marsh-McBirney sphere (NOIC, 1975); and those obtained from data published by McBirney, 1976. Our measurements, for two directions of flow, are also shown.

The NOIC data, and one set of our data, show a region of decreasing sensitivity for $5.10^4 < R < 8.10^4$. This is not evident in either the March-McBirney data or our second set and it cannot be accounted for by Cushing's analysis. This range of Reynolds numbers is well below the value at which transition to turbulent flow may be expected. It is also below the region of increased noise, remarked above. A series of observations were made as for the discus head using dye solution injected into the boundary layer near the forward stagnation point on a full scale model of the spherical head. The symmetry of the head and consequent lack of constraint on the path taken by the dye made these observations difficult; nevertheless it was possible to demonstrate the absence of transition below 1 m/sec.

4. AZIMUTH RESPONSE

The response to uniform flow in the plane of the electrodes was measured for each of the heads: for the annulus and sphere at three speeds, 10, 60 and 120 cm/s: at 15 and 170 cm/s for the discus head. Deviations from uniform amplitude response $(V_x^2 + V_y^2)^{\frac{1}{2}}$, error in resolved angle $\theta = \tan^{-1}(V_y/V_x)$, and standard deviation from the mean output at each

*It is possible that the transition to turbulence may occur in this region due to vibration and its associated velocity fluctuations. Hoerner (1958) gives R_{crit} as $\sim 10^5$(75 cm/sec) for a fluctuation to mean velocity ratio of 4%.

angle, are plotted in Figs. 11-13. The behaviour did not change significantly with speed: data are therefore shown at one speed in each case.

Of the three heads the discus (Fig. 12) had the most uniform response: with an amplitude error $\lesssim 0.8\%$ and angular error $<1^{\circ}$. These values are comparable with the accuracy of measurement. For the annulus (Fig. 11), departures from uniformity of response were $\lesssim 4\%$ and $\lesssim 4^{\circ}$, minimum output being obtained when the electrode axes are aligned along and across the tank. A change in output with azimuth may result from two causes: impediment of the flow by the four coil support struts and the change in wake pattern sampled by a pair of electrodes as the head is rotated. A rough estimate of the latter effect was made, using experimental data published by Schlichting for the wake defect behind a flat plate, and averaging the wake along the lines between electrodes. This produced an error distribution similar to that shown in Fig. 11 but nearly an order smaller. The coil and electrode support struts thus seem the most likely cause.

The sphere with 0.15 cm electrode protrusion exhibited the greatest deviation from uniformity (Fig. 13), at times approaching 18%. In most cases the sensor had greatest sensitivity when axes were aligned with the flow and perpendicular to it. Unexpectedly, in view of the symmetry about a vertical axis, the error appeared to vary between quadrants, particularly in the case of the 1.0 cm electrode protrusion. A similar effect is apparent in graphs published by the NOIC relating to a 4 inch diameter sensor. Fig. 14 is a comparison of the sphere azimuth response (first quadrant) with the response calculated for both axes from Cushing's equations, assuming that the "boundary layer coefficient", $C_B = -3$. Although the sign of the effect is correctly predicted, a value considerably less than -3 is required. The steady improvement in azimuth response with higher Reynolds numbers predicted by the equations is only partly realised in practice, agreement with theory being worse at higher azimuth angles.

5. TILT RESPONSE

In practice the current meter support in a mooring would contain a form of gimbal to maintain the sensor vertical. Nevertheless it is desirable to know the extent to which a cosine response is obtained in the vertical plane in the absence of any such arrangement. Measurements were therefore made at constant speeds with the annular and spherical heads inclined from the vertical (Figs. 15-17, 19 and 20). Angles were set to within $\pm 2^{\circ}$ using an inclinometer. The tilt response of the discus head had been investigated previously (Tucker, 1972) and this is reproduced in Fig. 18 for

comparison.

The response of the annular head was obtained at azimuth settings $\theta = 0^{\circ}$ and 45°, and for opposing directions of flow. With the sensor tilted into the flow the deviation from the ideal cosine dependence was greatest (~6%) at a tilt angle $\phi \simeq 50^{\circ}$. In the reverse direction the wake of the mounting bracket became important for angles $\phi > 45^{\circ}$, and slightly greater deviations were recorded.

The response of the sphere (1.5 mm electrode protrusion only) was obtained at an azimuth setting $\theta = 45^{\circ}$. This showed both over- and under-sensitivity (<10%) at small tilt angles, dependent on flow direction. Noise levels were an order greater than those obtained for the annulus. The least satisfactory performance is that of the discus head, whose output is substantially reduced when flow is incident on the face opposite to that containing the electrodes.

6. DYNAMIC TESTS

The ability of a two axis sensor to resolve a component of flow in the plane of the electrodes while rejecting any component normal to this plane is particularly important in near-surface applications, where mean horizontal current can be an order or more lower than wave orbital velocities. It was not certain that the ability of the sensor to do this in accelerating flow regimes could be inferred from the "static" measurements described heretofore. Consequently a device was constructed to move the sensor at a constant angular speed in a vertical, circular path in the tank so as to simulate wave conditions (Fig. 4). (A similar but more powerful rig has been constructed by Kalvaitis (1978): this can also be used to impart simple harmonic motion in one dimension, either vertically or horizontally).

It proved difficult to design and build an apparatus free from vibration. An accelerometer was therefore strapped to the stem of the sensor head, mounted coaxially with one axis of the current meter. The output was integrated and provided a means of distinguishing mechanically induced noise.

Fig. 21 shows the responses of each of the three types of head, obtained in each case from the first cycle of rotation in still water. Thereafter the response was degraded by up to 10% of the peak velocity. We attributed this to the previous passage through the water of the sensor head and its support stem.

The annulus and sphere have outputs that are clearly close to the ideal cosine response shown by the full line. The response of the discus head

is much poorer, particularly for $30^{\circ} < \phi < 210^{\circ}$, where the body of the sensor obstructs the flow. For $180^{\circ} < \phi < 360^{\circ}$, the flow is incident on the face containing the electrodes, and the correspondence with the cosine function is better, though not as good as the static measurements suggest. Fig. 21 contains a sequence of photographs taken at 25° intervals round a cycle (diameter 0.5 m: period 10 sec) of the orbital simulator, during which dye was ejected from a discus head. The direction of flow is shown alongside in each case and the angle follows the definition in Fig. 21 to aid comparison. The runs were made at different times with different heads, but the major features in both Figs. 21 and 22 were found to be reproducible. Note particularly the onset of the 'stall' condition at (f), which generates a large vortex (g) and (h). The consequent reversed flow component in the horizontal plane near the electrodes is evident in (h). Generally the direction taken by the dye plume corresponds quite well with the incident flow angle. This correspondence is not found in (j), (k) and (l), due no doubt to the tendency for the head to impart to the water a local upward velocity dependent on its own vertical velocity component.

An experiment was also conducted in which simultaneous translational and rotational motions were imparted to the discus head. By making these of equal magnitude the trajectory of the head can be made cycloidal. The flow vector then oscillates such that $0 < \phi < 180^{\circ}$ and the head always moves in undisturbed water. A polar plot is the most convenient method of presenting these results, which are compared in Fig. 23 with those for zero translational motion (abstracted from Fig. 21(c)), static tilt measurements (Fig. 18) and the ideal cosine response. Note that the 'stall' condition does not take place immediately flow is incident from behind the sensor: circulation takes place across the electrode face for 25°-30° beyond this point. Furthermore the loss of output is more sudden in the case of the static tilt observations. Increasing angle (counter-clockwise) then gives reversed output when $V_{trans} = 0$, before gradual recovery takes place. The output is not fully restored until $\phi = 186^{\circ}$. This delayed recovery, and the general asymmetry about the 90°-270° axis, show that the dynamic response does indeed differ considerably from the symmetrical response expected from static tilt measurements. This may be considered to result from the fact that the time taken to establish a flow regime around the body represents a significant fraction of the orbital period. The measurements described here are idealized and it is not clear how important - or unimportant - are these distortions of the vertical

cosine response in practice. Neither is it clear how data can be subsequently corrected for the effects of a distorted response. It seems reasonable to suppose, on the other hand, that if a good cosine response is obtained in the laboratory then errors incurred in the sea will be small.

7. STABILITY

The stability of a current sensor with time and in the presence of temperature changes can be important, particularly if it is required to extract weak residual currents from a time series of data. There are several potential sources of instability in electromagnetic current meters: zero drift in the d.c. amplifiers, contamination of the electrode surfaces, fouling of surfaces near the electrodes, and changes in the resistance between the coil and the seawater. With careful design, the first of these can be made very small. The second dictates a need for care when making laboratory measurements. Heads are handled frequently and pass through water surfaces which often carry a thin film of grease and dust. However, this does not appear to cause any difficulties in measurements at sea.

Gross errors can be caused by biological fouling of the sensor head since the boundary layer close to the electrodes is important in determining the head sensitivity. The effect is difficult to quantify because fouling rates are highly variable, in time as well as in geographical distribution. Apart from one or two specific instances - e.g. deployment from a drilling rig in the North Sea - this has not been a problem in work at IOS. The annular head may in fact prove less susceptible to errors caused by small amounts of fouling by virtue of its open construction: as yet no tests have been made of this, however.

Changes in the resistance between the coil and the seawater (and of the insulation resistance of associated cabling) affect the zero stability of the sensor. The coil-seawater resistance path forms a potential divider with the electrode source resistance, thus permitting a proportion of the coil drive voltage to appear at the electrodes. Provided this does not change, the constant offset thereby produced can be backed off. Typically the source resistance is 200 ohms, in parallel with a capacitance of $\sim 5\mu F$. The coil drive signal is 12 volts, and input sensitivity is 100 $\mu V/m/sec$. Thus a 50% change in insulation resistance (10^9 ohms) produces a zero shift of 3 cm/sec. In this respect the design of the annulus is the most critical, since a compromise has to be sought between a high, stable insulation resistance and a thin streamline form for the ring.

Some tests have been made of the stability with time of the discus head and an early version of the annular head. These are shown in Figs. 24 and 25. The discus head (one axis only) was tested in still, temperature controlled fresh water; if attributable to changes in insulation resistance the drift in sea water would be ~15 times lower due to the reduced source resistance. The annular head was similarly tested but in salt water of conductivity ~4S/m. On making an observation, each axis was shorted in turn, and a nominal correction was derived for drift in the amplifiers. The changes in head properties are thus shown separately from the drift in the complete current meter. Note that each axis shows a rapid initial change and then changes more slowly. The initial change is believed to be an electrode surface effect.*

The effect of temperature on the offset of the discus head in fresh water was measured between 1^{o} and 25^{o}C: a change in zero of ~1 cm/sec was observed in this interval. This is of the same order as the stability of the electronics unit.

8. CONCLUSION

The present measurements have shown that none of the three head designs tested is ideal, and that the type of head should be selected according to application. Thus for situations in which flow relative to the head is predominantly two dimensional the discus head has the best characteristics, but it seriously obstructs the flow whenever this is three dimensional - as in the surface wave field, or where there is appreciable mooring motion. The nature of the flow around a more bluff body like a sphere presents both advantages and disadvantages: the symmetry produces a much better vertical cosine response than in the case of the discus, but the earlier flow separation produces greater non linearity and noise level, and a poorer response in the plane of the electrodes. These effects are substantially reduced by greater electrode protrusion, but are unlikely to be eliminated entirely. The alternative method - to present as little obstruction as possible - still suffers from a degree of flow obstruction by coil supports, and it is less easily constructed than a 'solid' head. Nevertheless on the basis of tests made so far we feel that it offers the best approach for electromagnetic current meter measurements in three dimensional flow.

ACKNOWLEDGEMENTS

We are grateful to J. Bunting for assistance with the current meter electronics, and to N.D. Smith for fabrication of the spherical sensor.

The work was commissioned by the Departments of Industry and Energy.

*A 2000 hour fresh water stability test has since been made on the annular head. The changes in zero output were less than ±0.7 cm/sec.

REFERENCES

CUSHING, V. Electromagnetic water current meter. Paper 25C, Proc. MTS-IEEE Conference 'Oceans '76'. Washington D.C., September 1976.

HOERNER, S.F. Fluid-Dynamic Drag. Published by the author, 1958.

IRISH, J.D. and M.D. LEVINE. Digitizing error from period and frequency counting techniques. Deep-Sea Research, Vol. 25, pp. 211-219, 1978.

KALVAITIS, A.N. The vertical planar motion mechanism: a dynamic test apparatus for evaluating current meters and other marine instrumentation. Report prepared for U.S. Environmental Protection Agency, No. EPA-600/7-78-145, July 1978.

KANWISHER, J. and K. LAWSON. Electromagnetic flow sensors. Limnology and Oceanography, Vol. 20(2), pp. 174-182, 1975.

McBIRNEY, T.R. Azimuth and tilt response of a spherical electromagnetic water velocity sensor. Tech. Note 2, Marsh-McBirney Inc., 2281 Lewis Avenue, Rockville, Maryland, U.S.A.

McBIRNEY, T.R. Development of an electromagnetic water velocity sensor with accurate angular responses. Advances in Instrumentation, Vol. 31, 13, 754, pp. 1-12, 1976.

NOIC. Report on Test and Evaluation of Four Ocean Current Measuring Systems. National Oceanographic Instrumentation Centre, Washington, October 1975.

SHERCLIFF, J.A. The Theory of Electromagnetic Flow Measurement. Cambridge University Press, 1962.

TUCKER, M.J. Electromagnetic current meters. An assessment of their problems and potentialities. Proc. SUT, Vol. 2, No. 1, pp. 53-58, 1972.

TUCKER, M.J., N.D. SMITH, F.E. PIERCE and E.P. COLLINS. A two-component electromagnetic ships log. J. Inst. Nav., Vol. 23, No. 3, pp. 302-316, July 1970.

Appendix 1 An approximation of the effect of the boundary layer on the sensitivity of the discus sensor

A calculation has been made of the likely order of the effect of boundary layer thickness variation with speed on the sensitivity of the discus sensor. The following restrictions and assumptions were made:

(1) The problem was reduced to two dimensions by considering the plane in line with a pair of electrodes and normal to the discus surface. The computation was then made over one half of this plane, as the problem is symmetrical.

(2) The boundary layer thickness and velocity profile were assumed to be those of a flat plate when flow is incident in the plane of the plate.

Theory of the calculation

Bevir (1970) gives the voltage difference between a pair of electrodes in a magnetic field B as:

$$u_1 - u_2 = \int \underset{\sim}{v}.(\underset{\sim}{B} \times \underset{\sim}{j})d\tau \qquad (1)$$

u_1, u_2 = voltages at electrodes 1, 2
$\underset{\sim}{v}$ = fluid velocity
$\underset{\sim}{B}$ = magnetic flux density
$\underset{\sim}{j}$ = virtual current vector
τ = flowmeter volume

The virtual current vector $\underset{\sim}{j}$ can be written as gradF where F is a solution to Laplace's equation for an unit current source at electrode 1 and an unit current sink at electrode 2.

Expanding equation 1 gives:

$$u_1 - u_2 = \int v_x(j_yB_z - j_zB_y) - v_y(j_xB_z - j_zB_x) + v_z(j_yB_x - j_xB_y)d\tau \qquad (2)$$

From Fig.A1 $v_x = v_y = 0$

therefore: $$u_1 - u_2 = \int v_z(j_yB_x - j_xB_y)d\tau \qquad (3)$$

Fig.A1. Diagram of discus axes

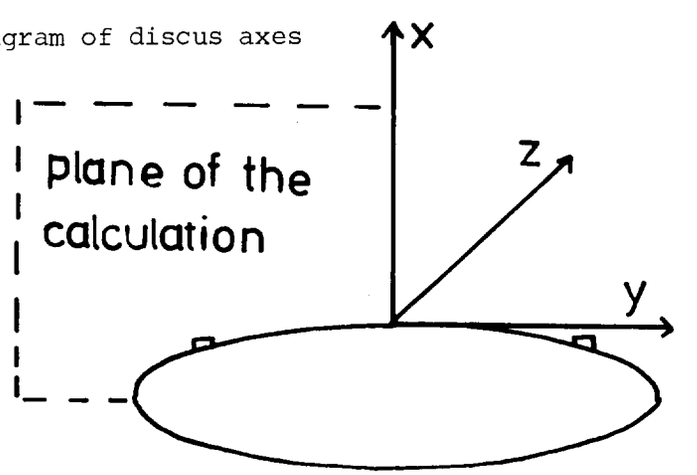

Calculation Procedure

(1) The solution to Laplace's equation, F, was obtained by a finite difference calculation on a grid 3.5L × 2.5L, where L is the electrode separation. The mesh size was $^1/_{20}$L, i.e. 4 mm. 350 iterations were made before the virtual current vector j = grad F was calculated. It was assumed that F = 0 at the grid boundaries.

(2) Measurement of the magnetic flux density B of the sensor was made using a magnetodiode, on a 4 mm grid in the x and y directions.

(3) Using the measured B and the calculated j, the weighting function $(j_y B_x - B_x j_y)$ was calculated. A contour plot of this function is given in Fig. A2.

(4) A linear interpolation of the 4 mm grid onto a 1 mm mesh was made, so that thinner boundary layers could be examined.

(5) Velocity profiles were calculated on a flat plate assumption for the discus surface. The boundary layer thickness was found from Le Méhauté (1976):

$$\delta = 5.5x/(xU_o/v)^{\frac{1}{2}} \qquad (4)$$

δ = boundary layer thickness

x = distance behind leading edge of discus

U_o = free stream velocity

v = viscosity

and the velocity profile within the boundary layer:

$$\frac{u(y)}{U_o} = 2\left(\frac{Y}{\delta}\right) - \left(\frac{Y}{\delta}\right)^2 \qquad (5)$$

y = distance from the surface to a point in the boundary layer.

Elsewhere the velocity was given its free stream value.

(6) A summation was then made over an 8 cm by 3.5 cm area on the 1 mm mesh at fluid velocities of 1 cm/s to 25 cm/s (boundary layer thickness of 13 mm to 2.4 mm).

The potential difference thus calculated at each velocity has been converted to sensitivity (output/cm/sec) normalized to unity at 50 cm/sec. A plot of normalized sensitivity against velocity is shown in Fig. A3 (solid curve), together with the results of a series of measurements of the output from two discus sensors, similarly normalized.

The calculation based on boundary layer thickness thus correctly predicts the trend towards a reduction in sensitivity at low speeds, and its order of magnitude. Closer agreement cannot be expected in view of the simplifying assumptions made in the calculation. Note also that some measurements made with specially prepared electrodes protruding 1 cm from

the discus surface on insulated shanks show a tendency to delay the reduction. in sensitivity as velocity falls. This again is consistent with the surface boundary layer effects.

References

Bevir, M.K. The theory of induced voltage electromagnetic flowmeters. Journal of Fluid Mechanics, Vol. 43(3), pp. 577-590, 1970.

Le Méhauté, B. An Introduction to Hydrodynamics and Water Waves. Springer-Verlag, New York, 1976.

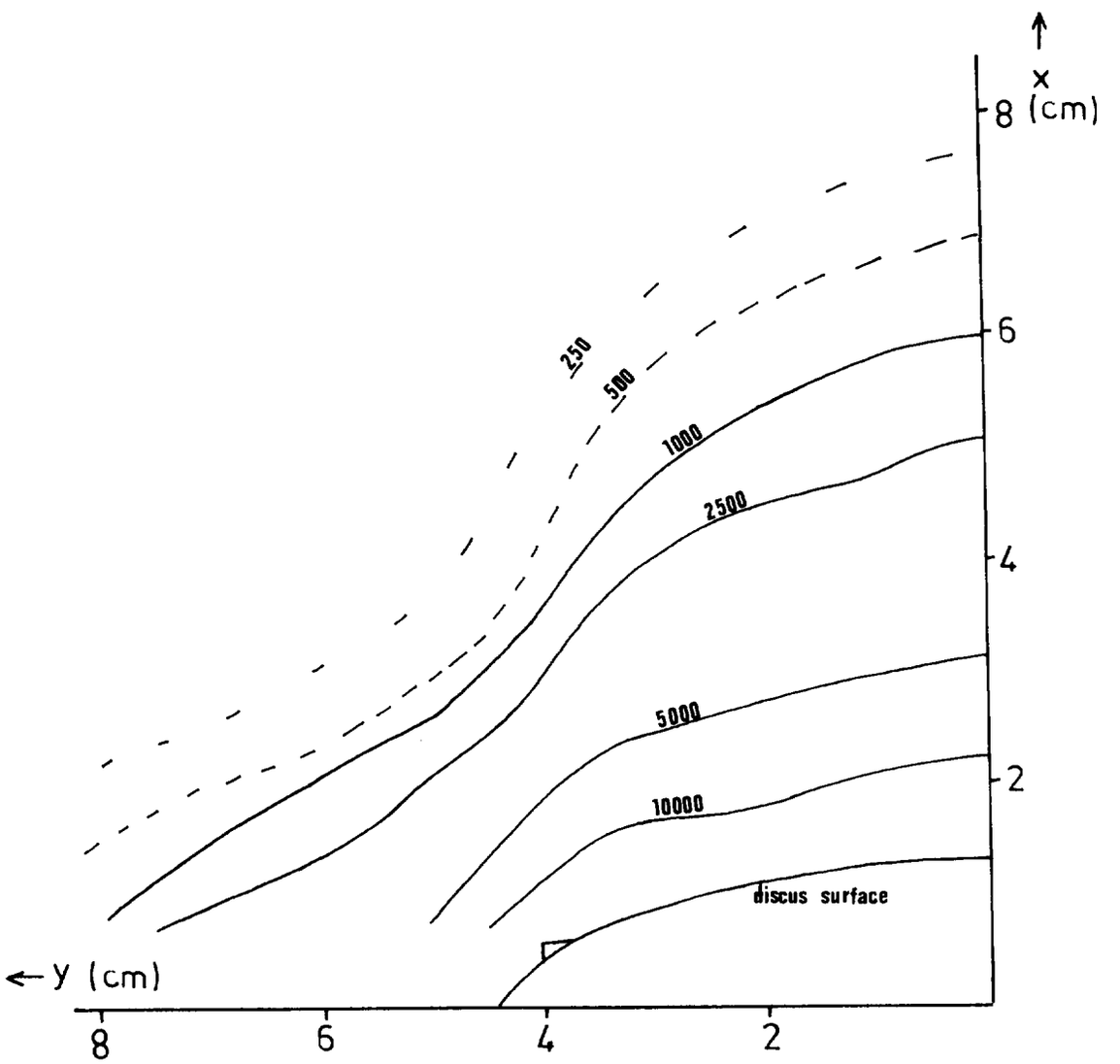

Fig. A2 Contour plot of the weighting function $(B_x j_y - B_y j_x)$.

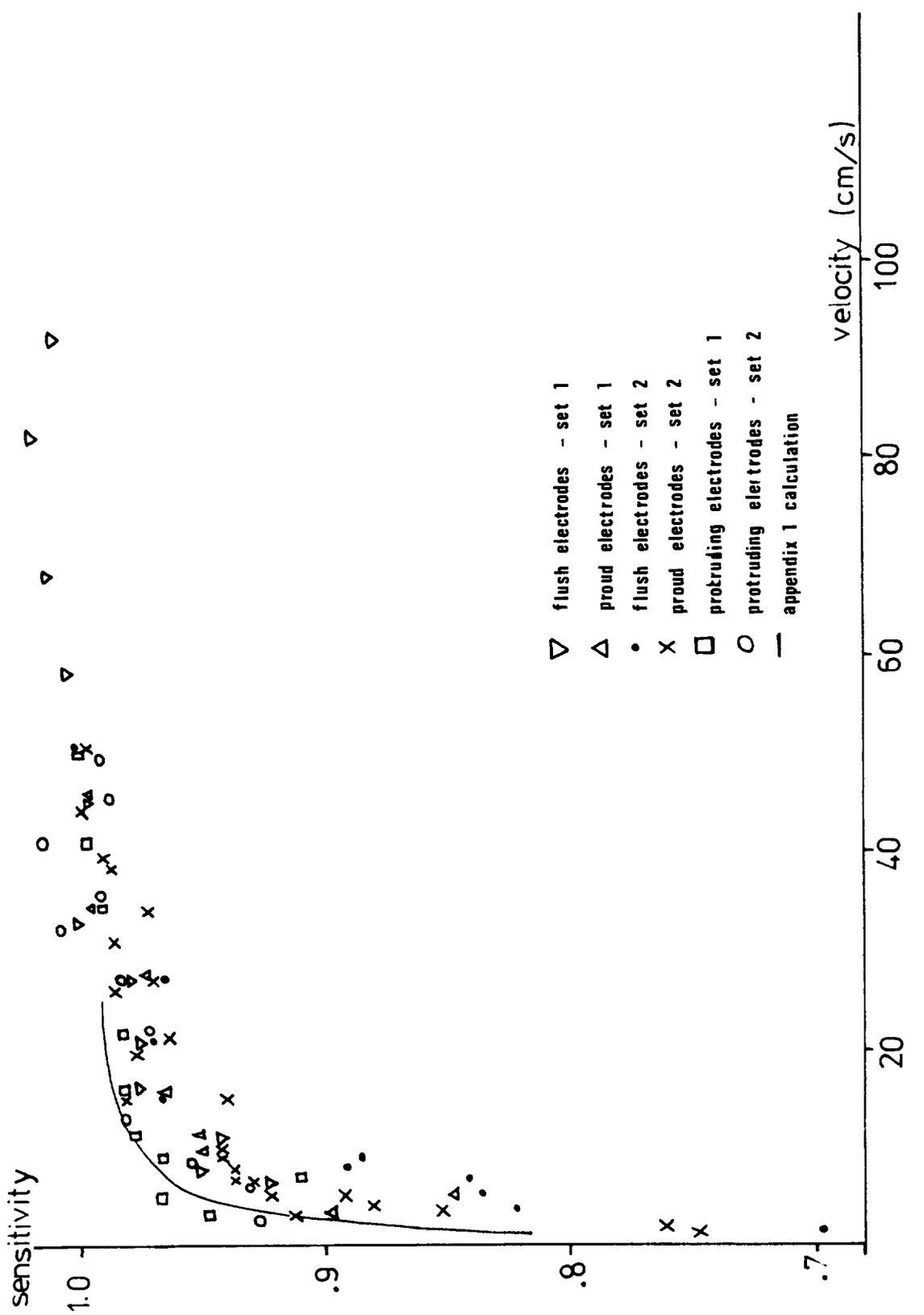

Fig.A3. Discus sensor sensitivity as a function of speed.

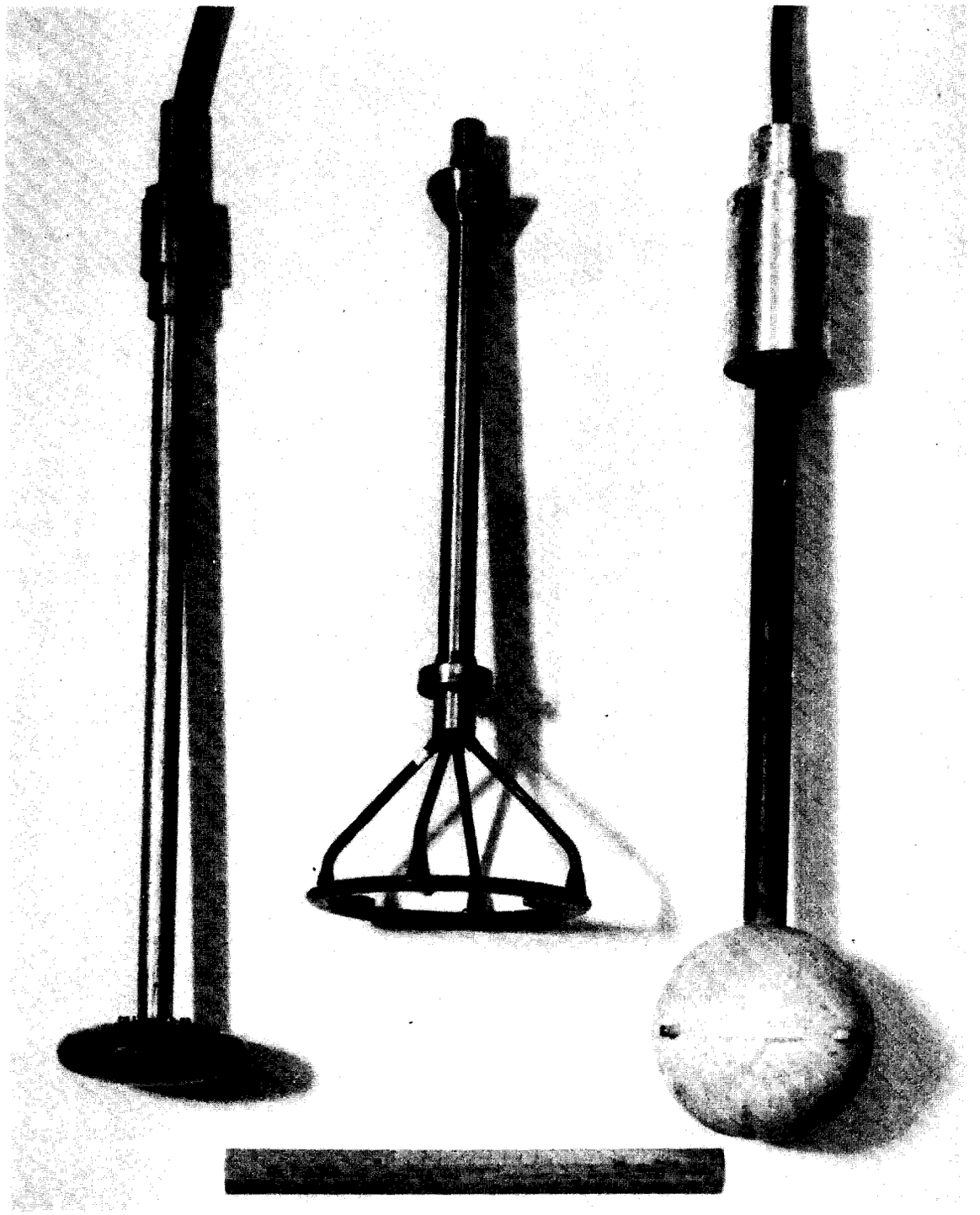

Fig. 1. Three types of electromagnetic current sensor on which tests were made. Left to right: discus head, annular head and sphere (1 cm electrode protrusion). Tests were made also on the sphere with 1.5 mm electrode protrusion.

a)

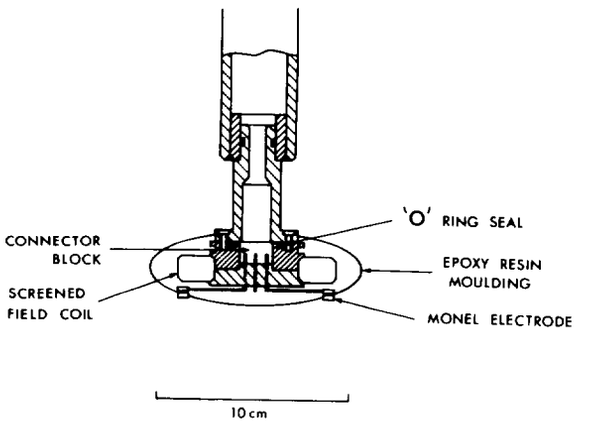

b)

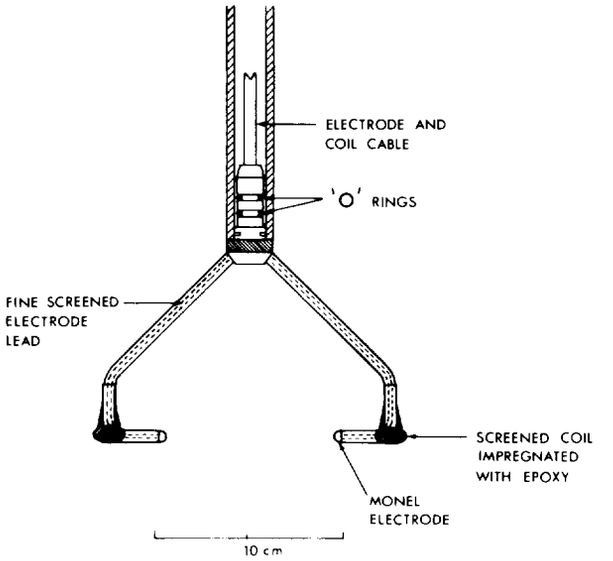

c)

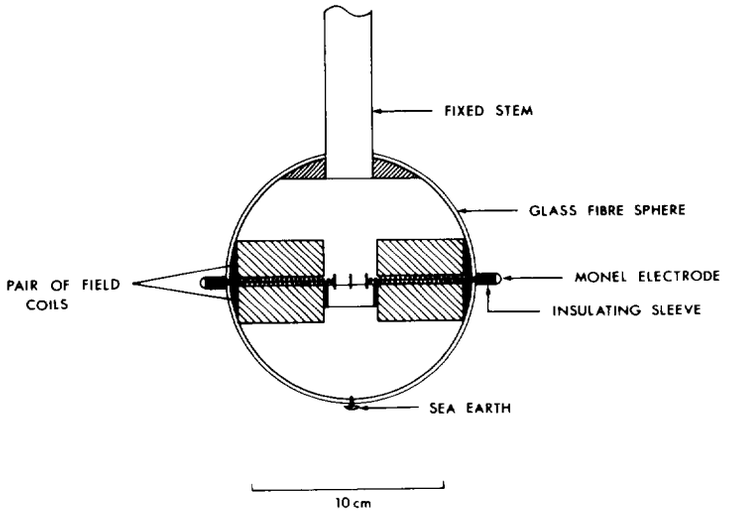

Fig. 2. Sectional views of the three head types.

(a) Discus

(b) Annulus

(c) Sphere

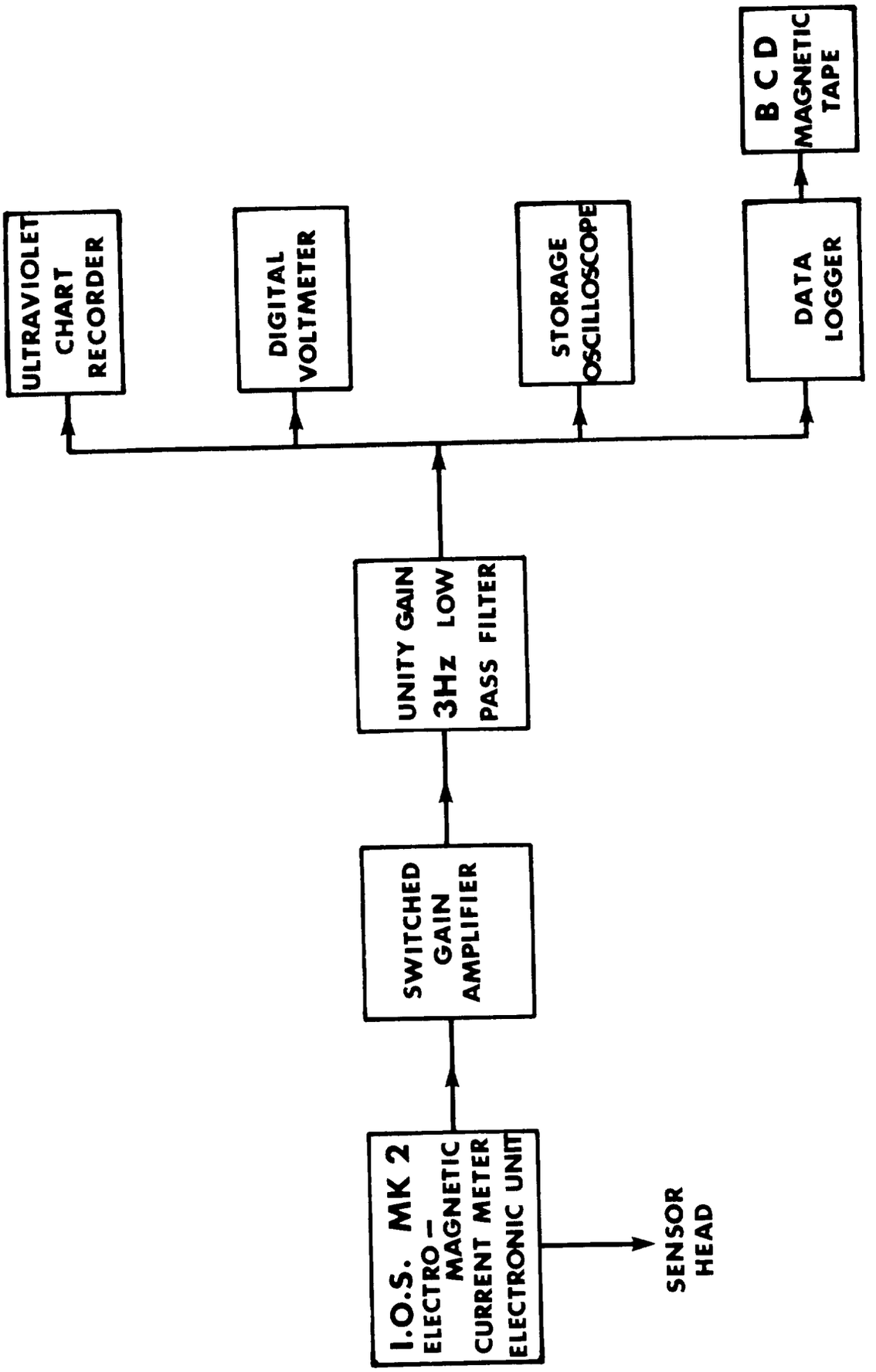

Fig. 3. Block schematic of measurement system.

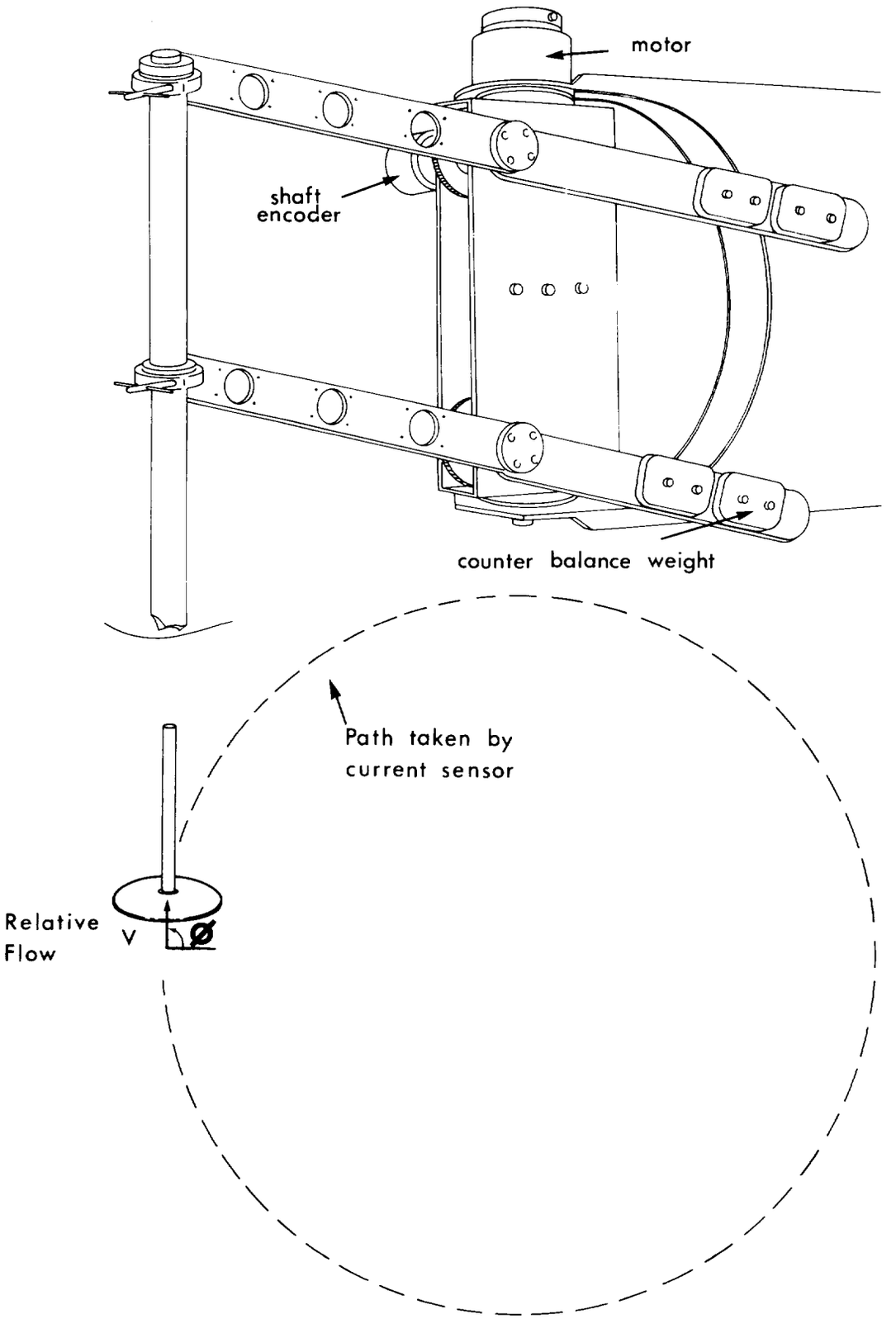

Fig. 4. Orbital motion simulator.

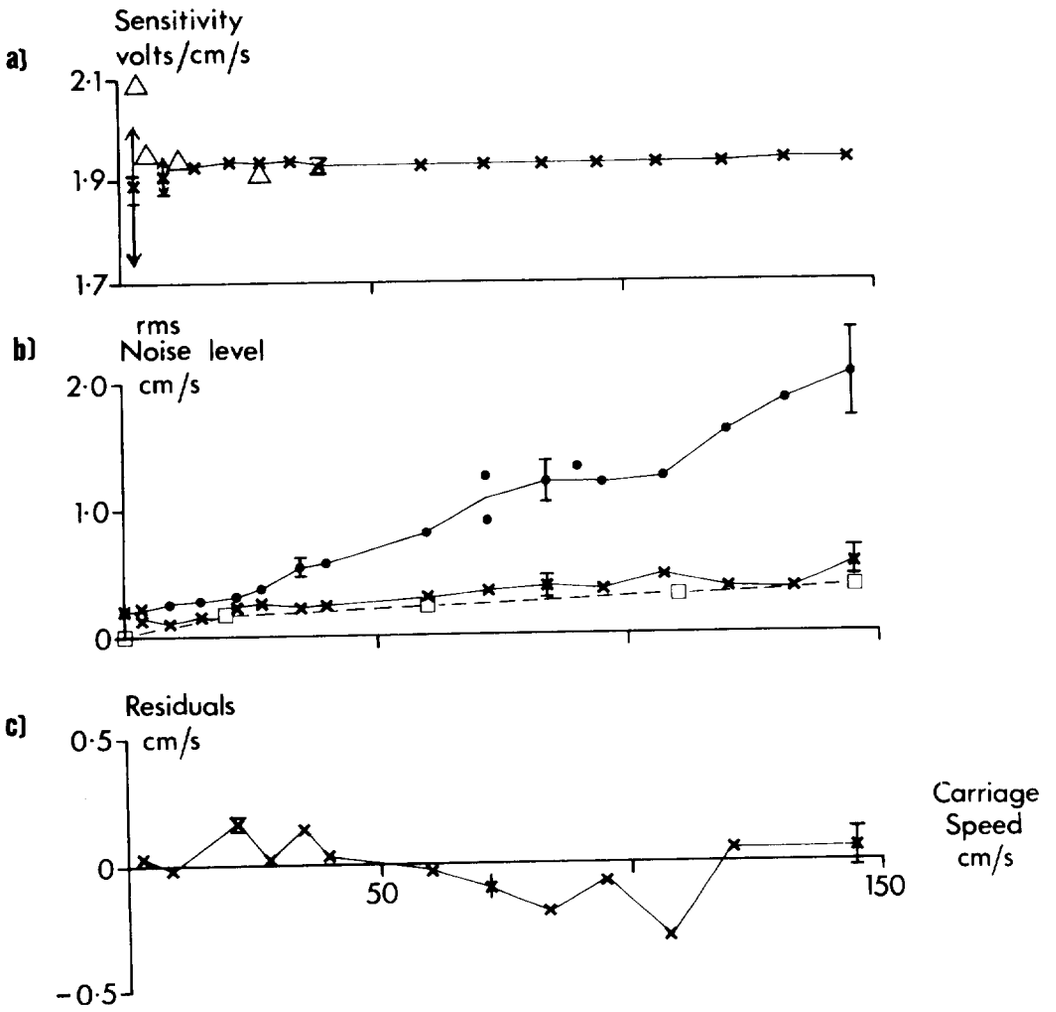

Fig. 5. Annulus: (a) Sensitivity (output/speed).
(b) R.m.s. noise level.
(c) Residuals (observations - best linear fit) plotted against speed.

× Measurement in flow direction (positive direction).

△ Measurement in flow direction (negative direction).

• Measurement normal to flow (transverse axis).

□ Standard deviation of carriage speed sensor readings.

I 95% confidence limits.

↕ ±2 mm/s uncertainty in residual flow in tank.

R.m.s. quantisation noise for each c.m. channel = 0.21 cm/s: for carriage speed = 0.165 cm/s. Note that quantisation noise for the carriage speed sensor is zero at rest since no pulses are output.

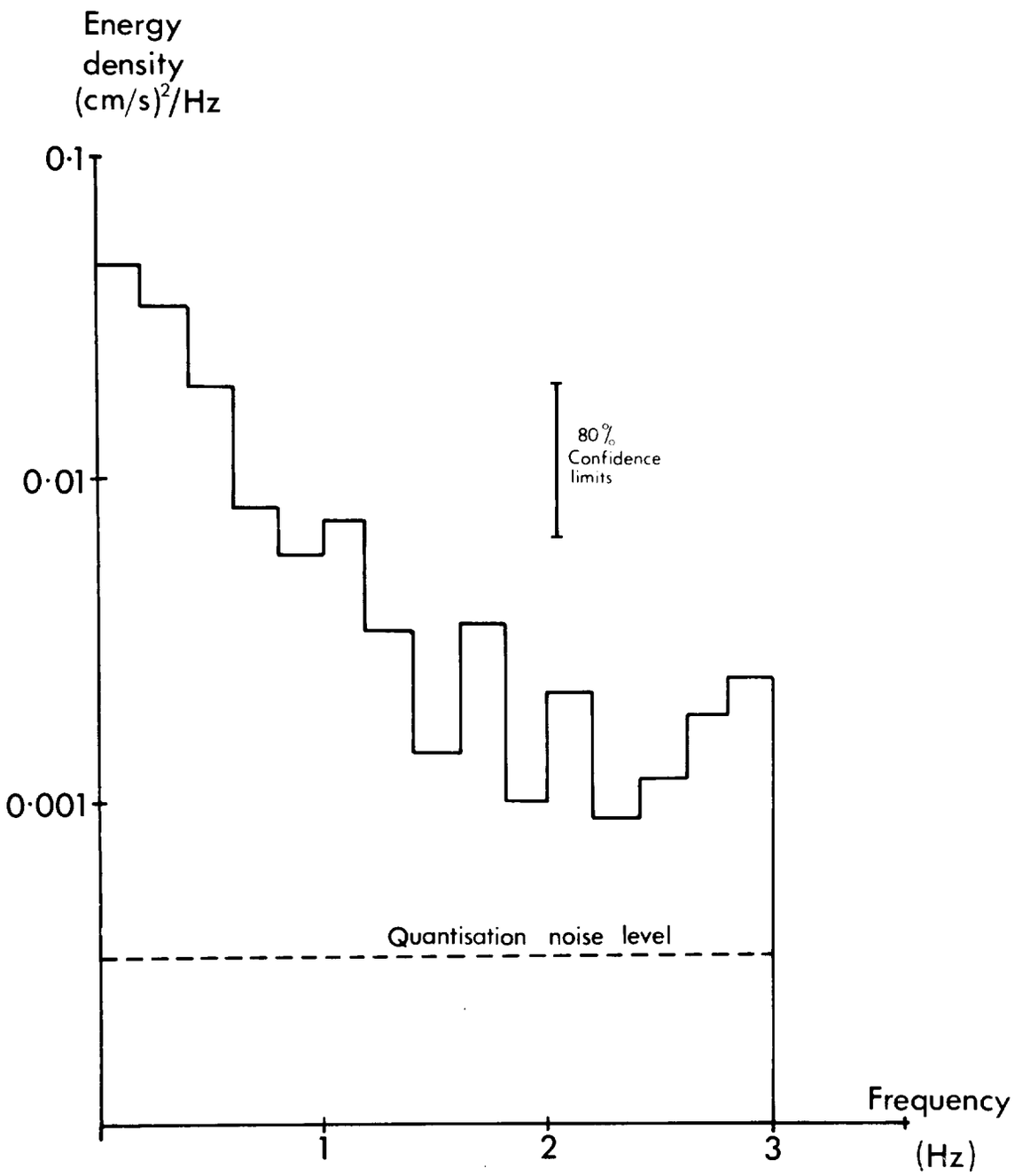

Fig. 6. Spectrum of noise obtained using annular head in laminar flow at 16 cm/s. Measurement axis in flow direction: flow in plane of annulus.

Fig. 7. Discus: (a) Sensitivity (output/speed).
(b) R.m.s. noise level.
(c) Residuals (observations - best linear fit) plotted against speed.

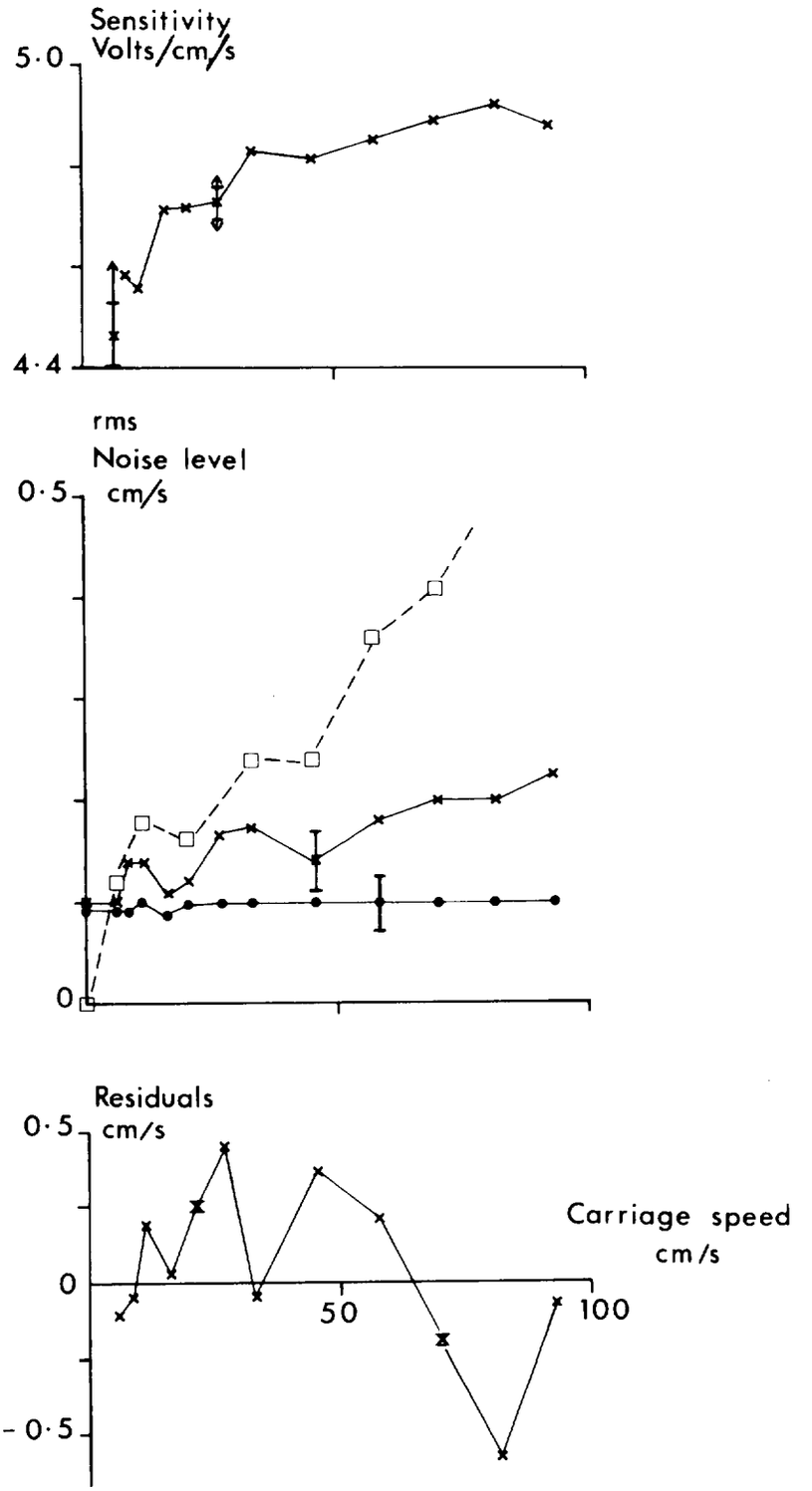

× Measurement in flow direction.

• Measurement normal to flow.

□ Standard deviation of carriage speed sensor readings.

I 95% confidence limits.

↕ Uncertainty due to residual flow = ±2 mm/s.

Quantisation noise for each c.m. channel and towing carriage speed indicator = 0.082 cm/s.

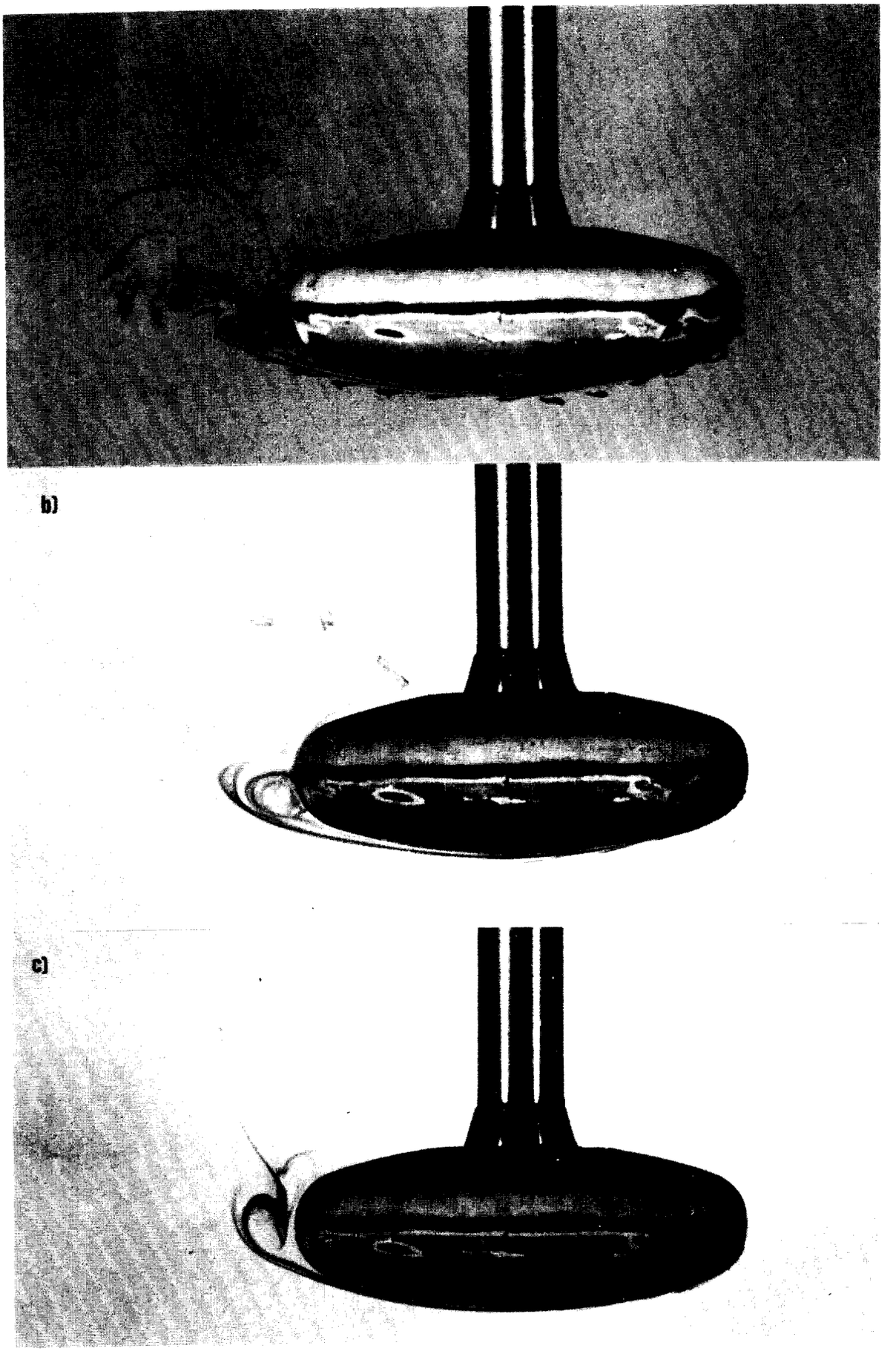

Fig. 8. Steady laminar flow around discus head (moving left to right).
(a) 1.8 cm/s. Note that flow is attached over virtually the
(b) 10.4 cm/s. entire head surface: separation takes place
(c) 10.4 cm/s. near the rear. The reverse flow region and consequent formation of a vortex can be seen clearly. Note also the effect of the stem wake.

Fig. 9. Sphere: (a) Sensitivity (output/speed).

(b) R.m.s. noise levels for axis in flow direction.

(c) Residuals (observations - best linear fit) plotted against speed.

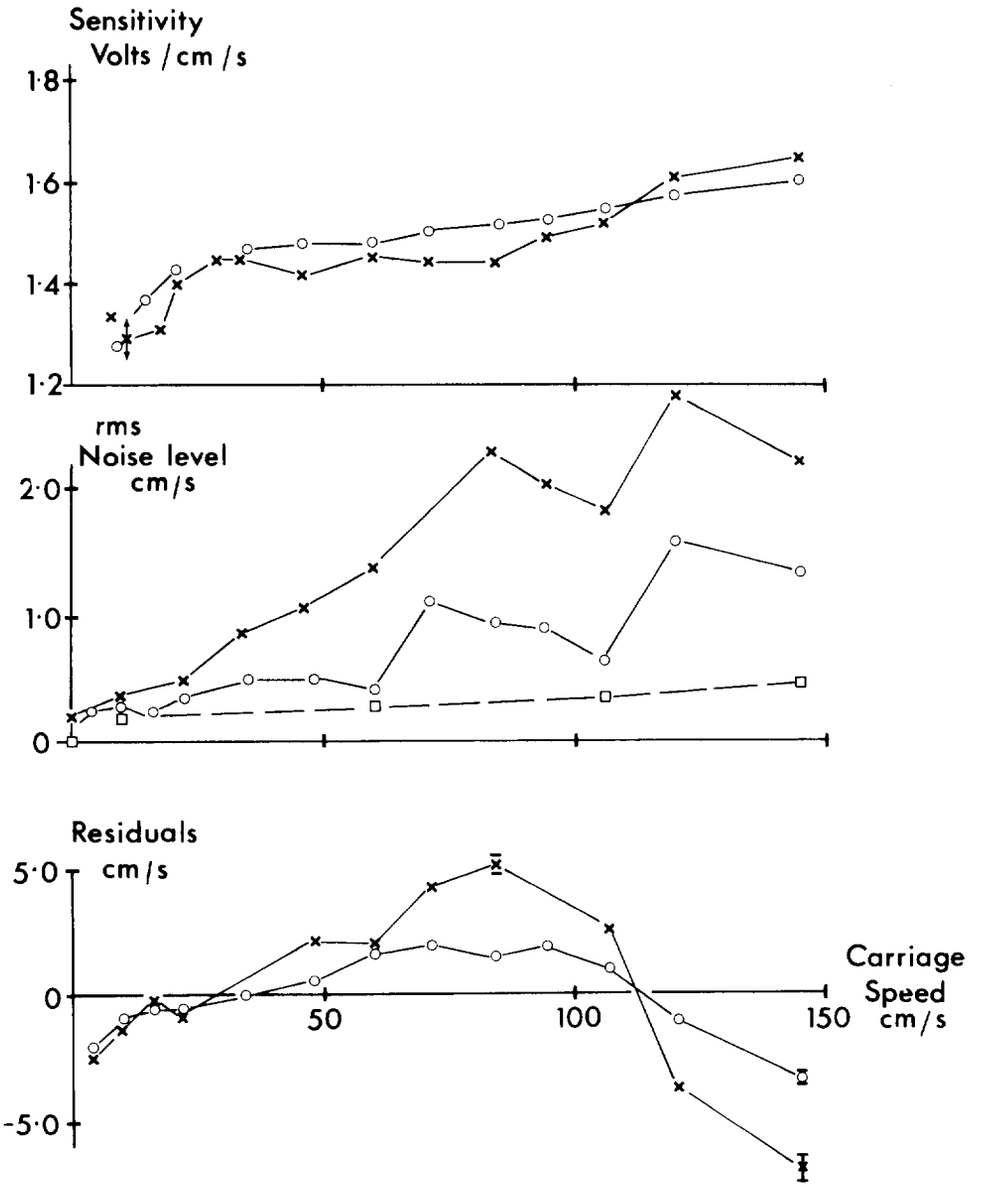

o 10 mm electrode protrusion.

× 1.5 mm electrode protrusion.

□ Standard deviation of carriage speed sensor readings.

I 95% confidence limits.

↕ ±2 mm/s uncertainty in residual flow in tank.

Note that noise levels relate to flow direction only. Noise in transverse axis was of similar magnitude. R.m.s. quantisation noise = 0.28 cm/s for c.m., = 0.165 for carriage speed.

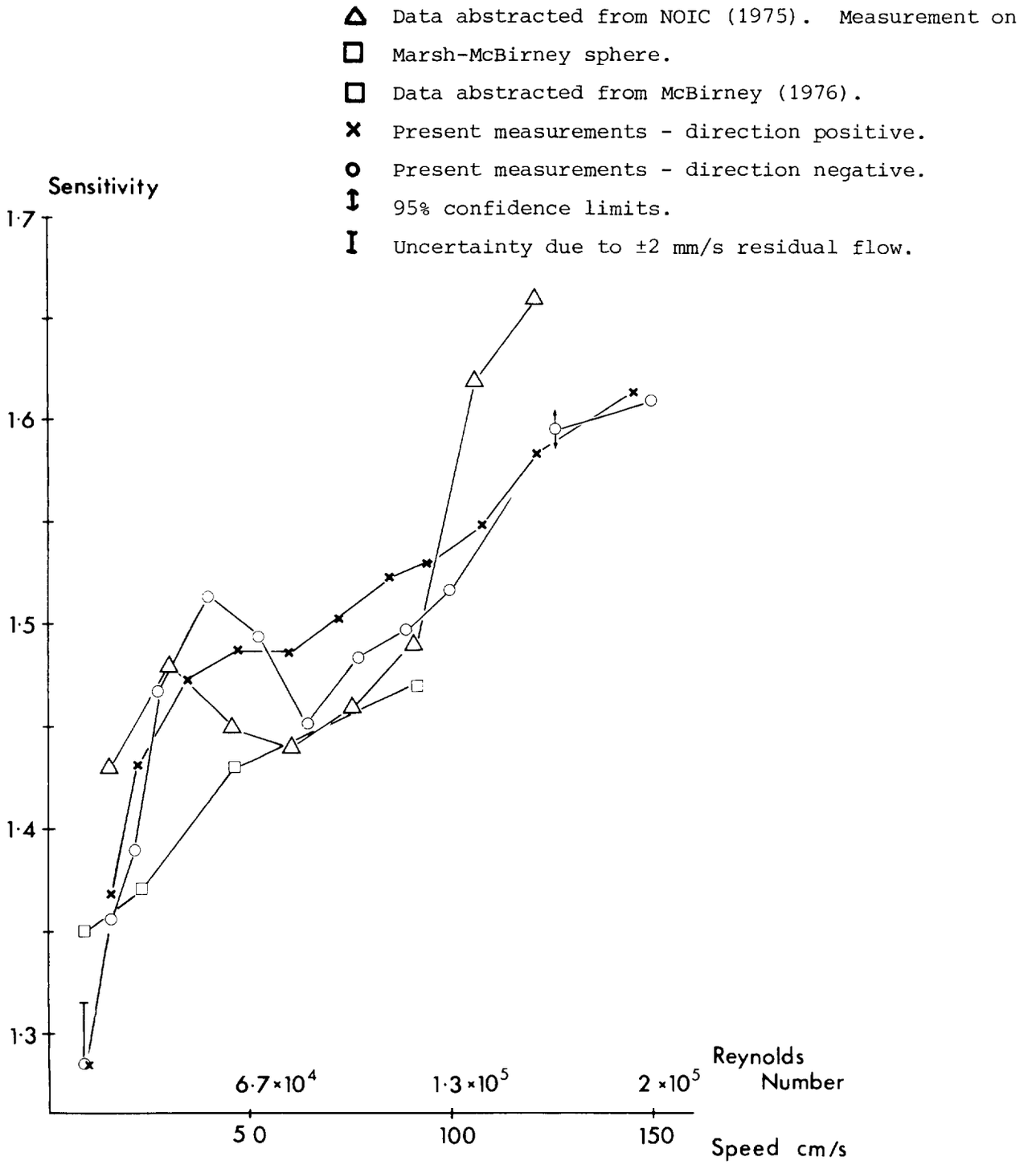

Fig. 10. Sensitivity plotted against speed for different types of spherical head. Data have been extracted from an NOIC report (NOIC, 1975) on a 4 inch diameter March-McBirney head, and from a publication by the manufacturer (Marsh-McBirney, 1975). Present measurements on the IOS experimental head are shown also.

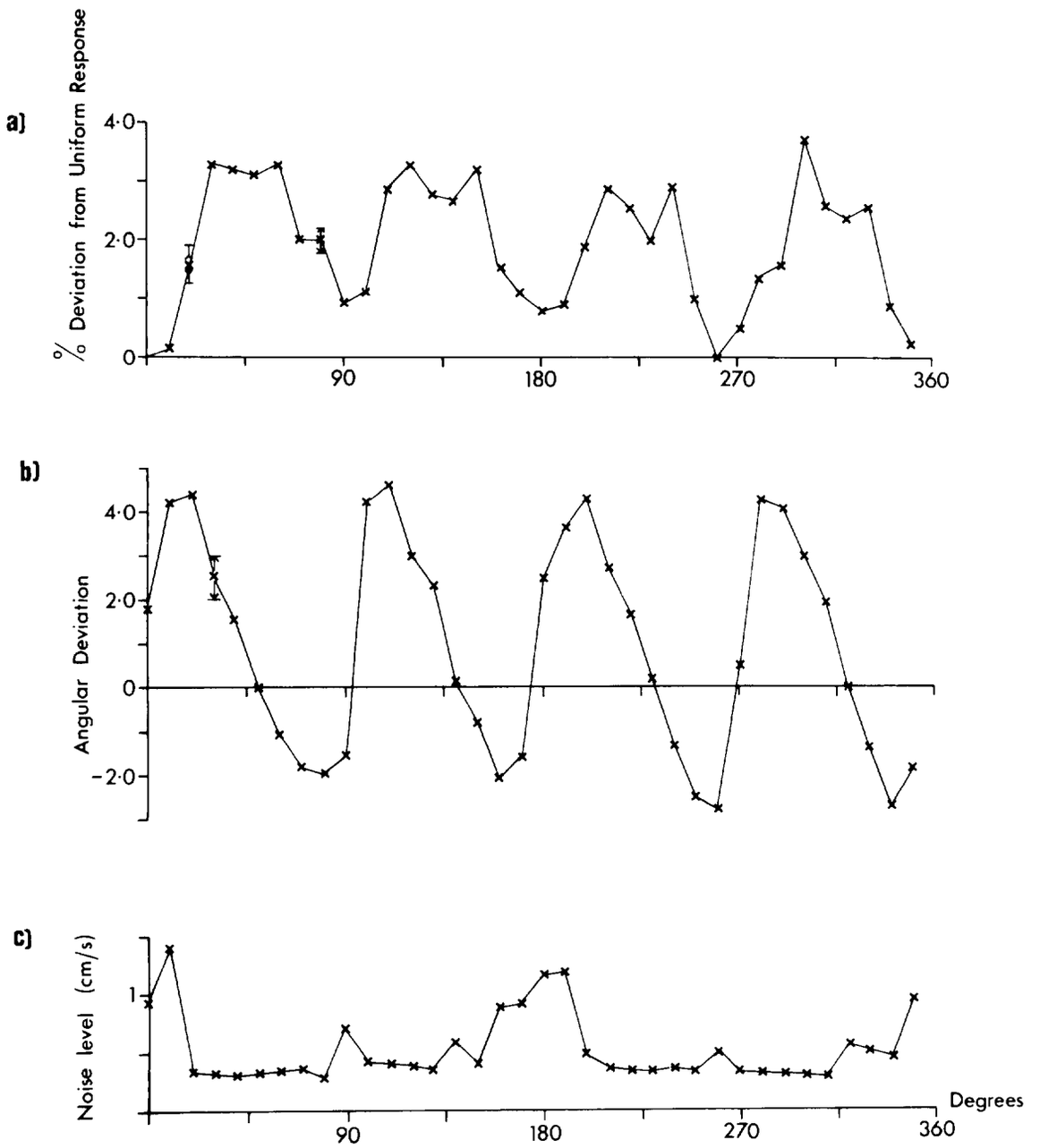

Fig. 11. Azimuth response of annular head: flow horizontal and coplanar with electrodes. Speed = 60 cm/s.

(a) Deviation from uniform response in magnitude.

(b) Angular error in degrees. Error bars denote 95% confidence interval.

(c) Standard deviations from mean outputs (noise).

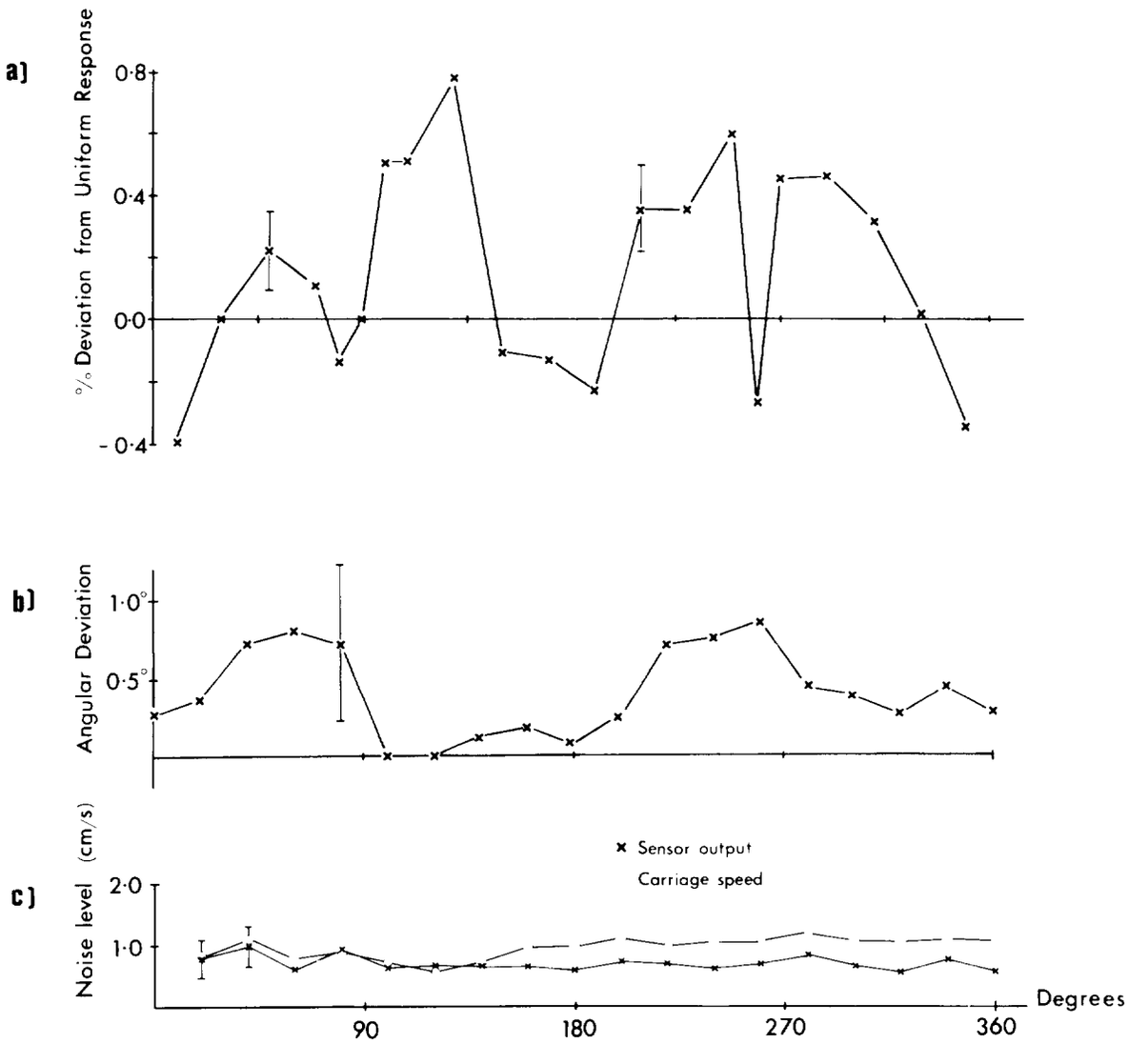

Fig. 12. Azimuth response of discus head: flow horizontal and coplanar with electrodes. Speed = 170 cm/s.

(a) Deviation from uniform response in magnitude.

(b) Angular error in degrees.

(c) Standard deviations from mean outputs (noise). Circular symbols show noise output from carriage speed sensor. Error bars denote 95% confidence interval.

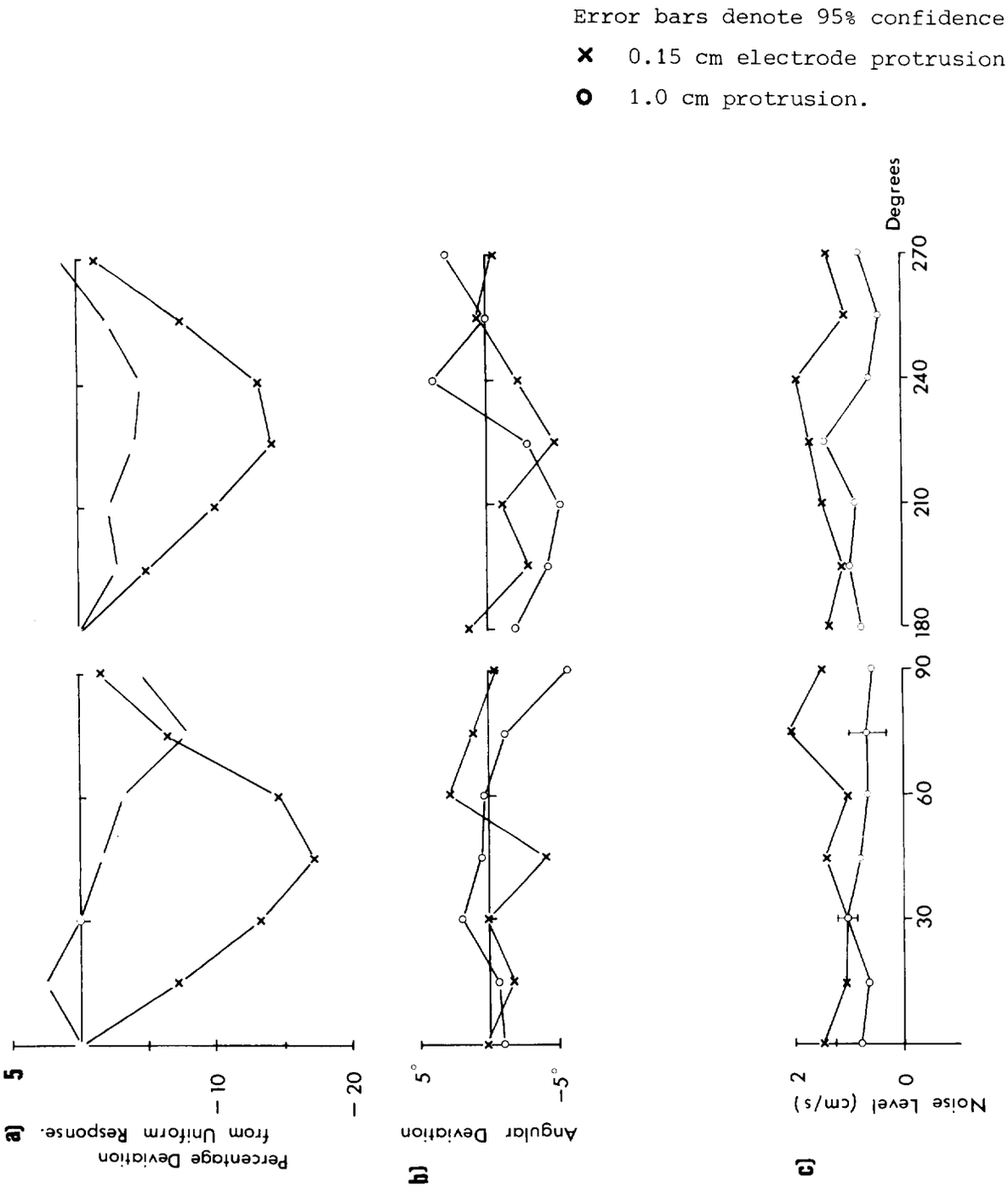

Fig. 13. Azimuth response of spherical head; flow horizontal and coplanar with electrodes. Measurements made in two quadrants only. Speed = 60 cm/sec.

(a) Deviation from uniform response in magnitude.

(b) Angular error in degrees.

(c) Standard deviations from mean outputs (noise).

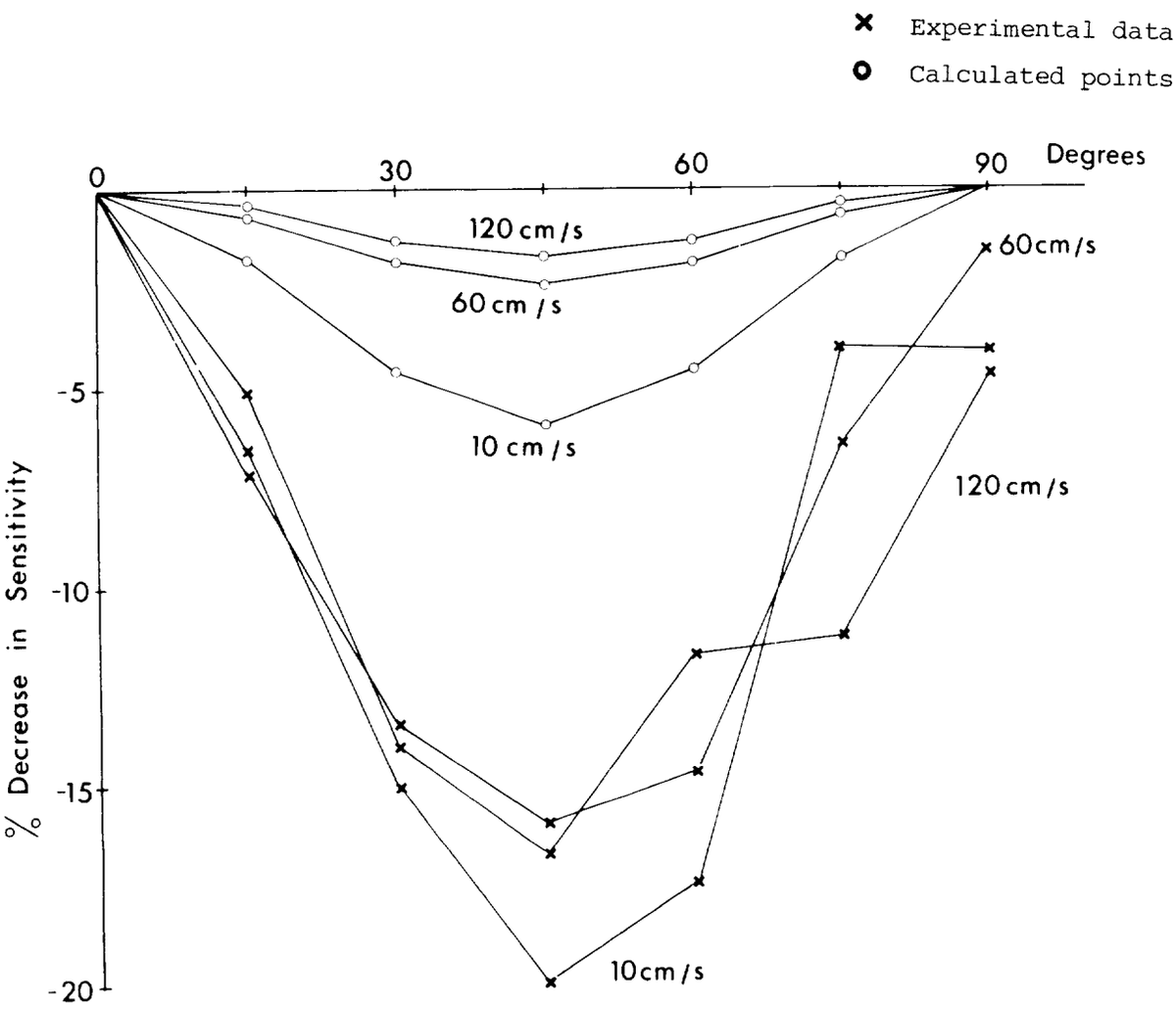

Fig. 14. Comparison of azimuth response of spherical head (electrode protrusion 0.15 cm) at three speeds with theoretical responses derived from Cushing (1976) analysis. Boundary layer coefficient assumed = -3.

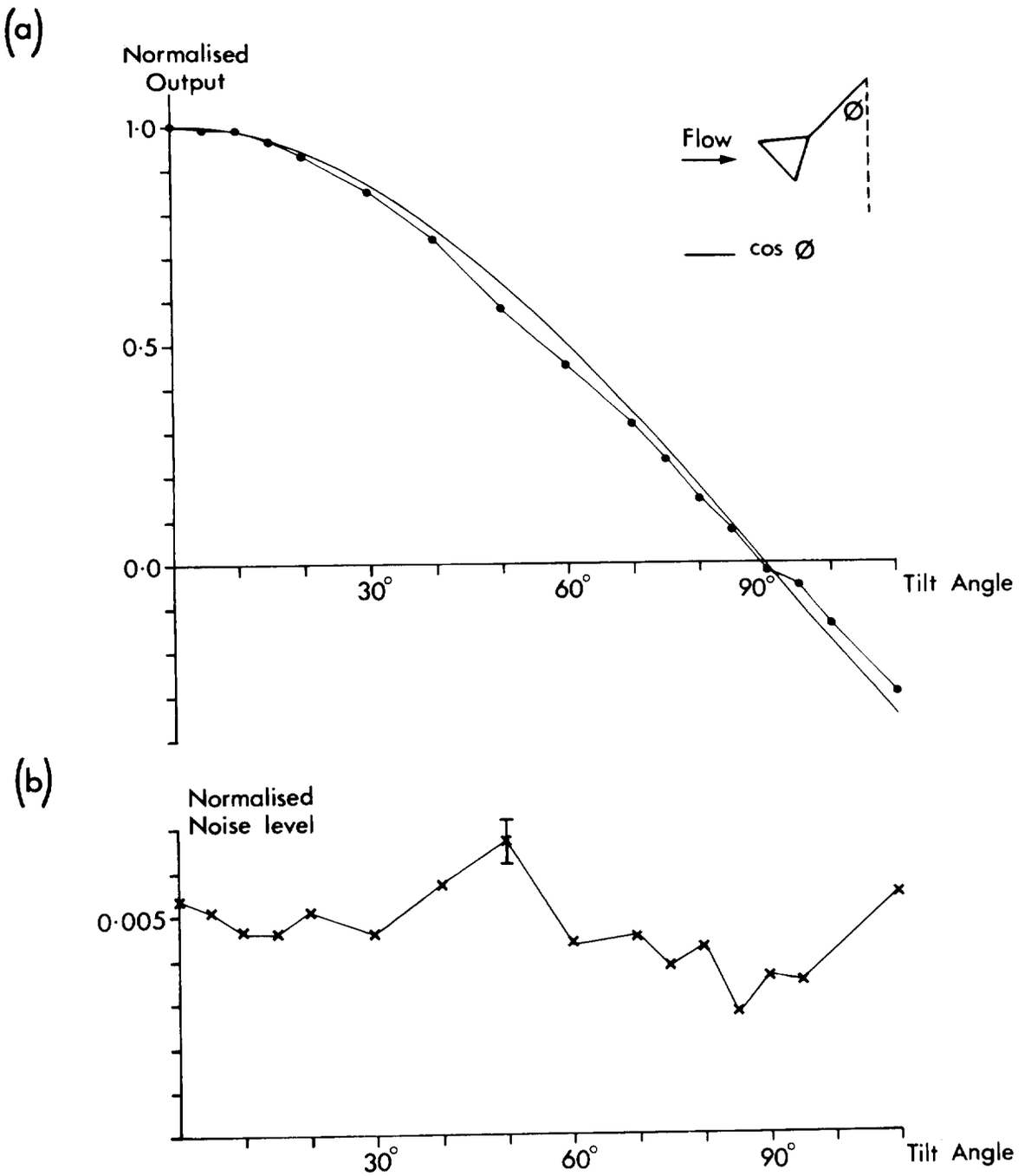

Fig. 15. (a) Response of annular head tilted from vertical mounting at fixed angle ϕ. Azimuth $\theta = 0^{\circ}$. Speed = 60 cm/s.

(b) Noise level expressed as a fraction of output at $\phi = 0^{\circ}$. Note that 95% confidence interval for (a) is therefore of same order as size of plotted symbol. Uncertainty in residual flow contributes negligible error.

95% confidence interval is of same order as size of plotted symbol. Maximum uncertainty (±0.02) due to residual flow occurs at small ϕ, and is negligible at $\phi = 90^{\circ}$.

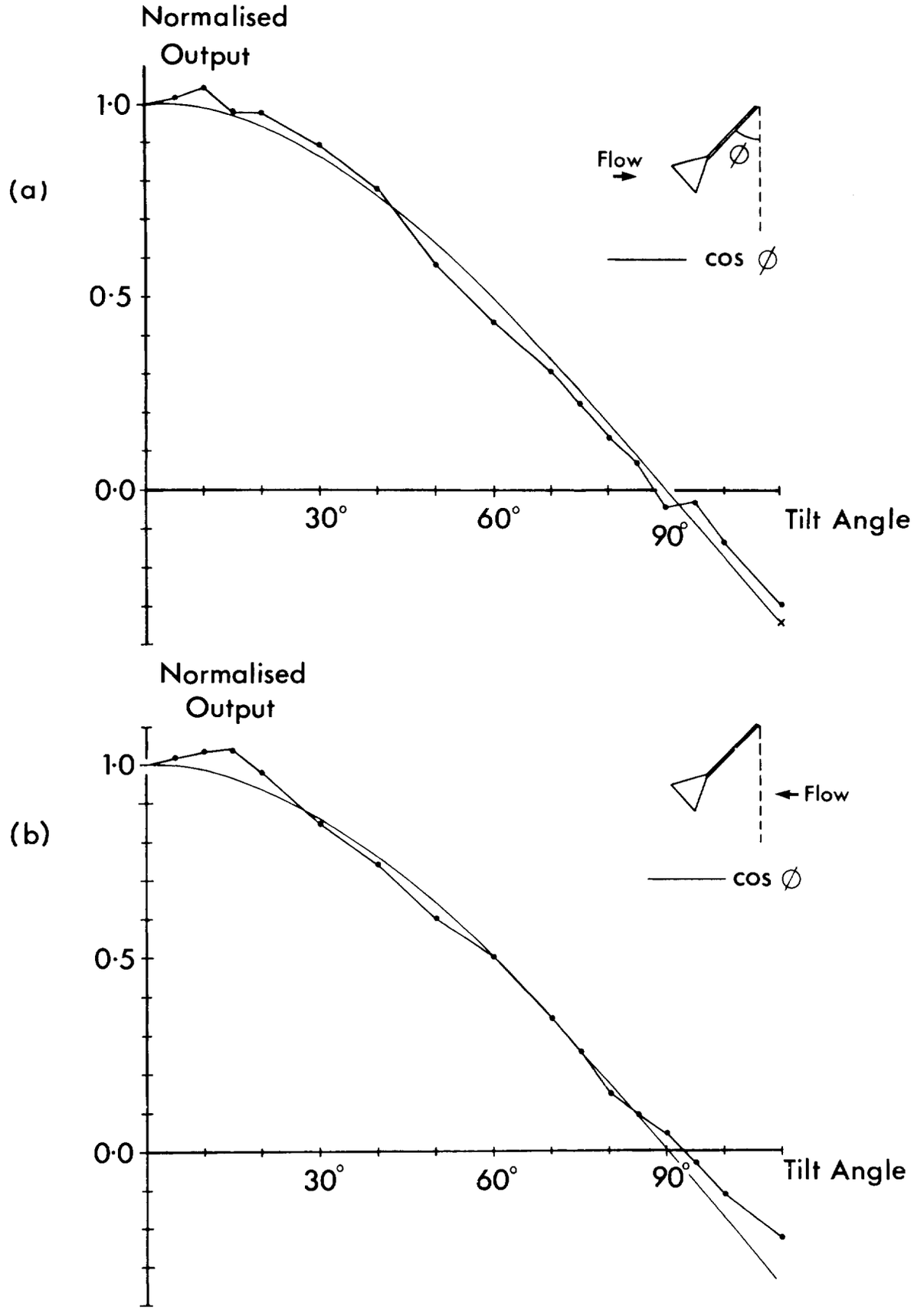

Fig. 16. Response of annular head tilted from vertical mounting at fixed angle ϕ. Azimuth $\theta = 0^{\circ}$. Speed = 12 cm/s.

(a) Positive flow direction.

(b) Negative flow direction.

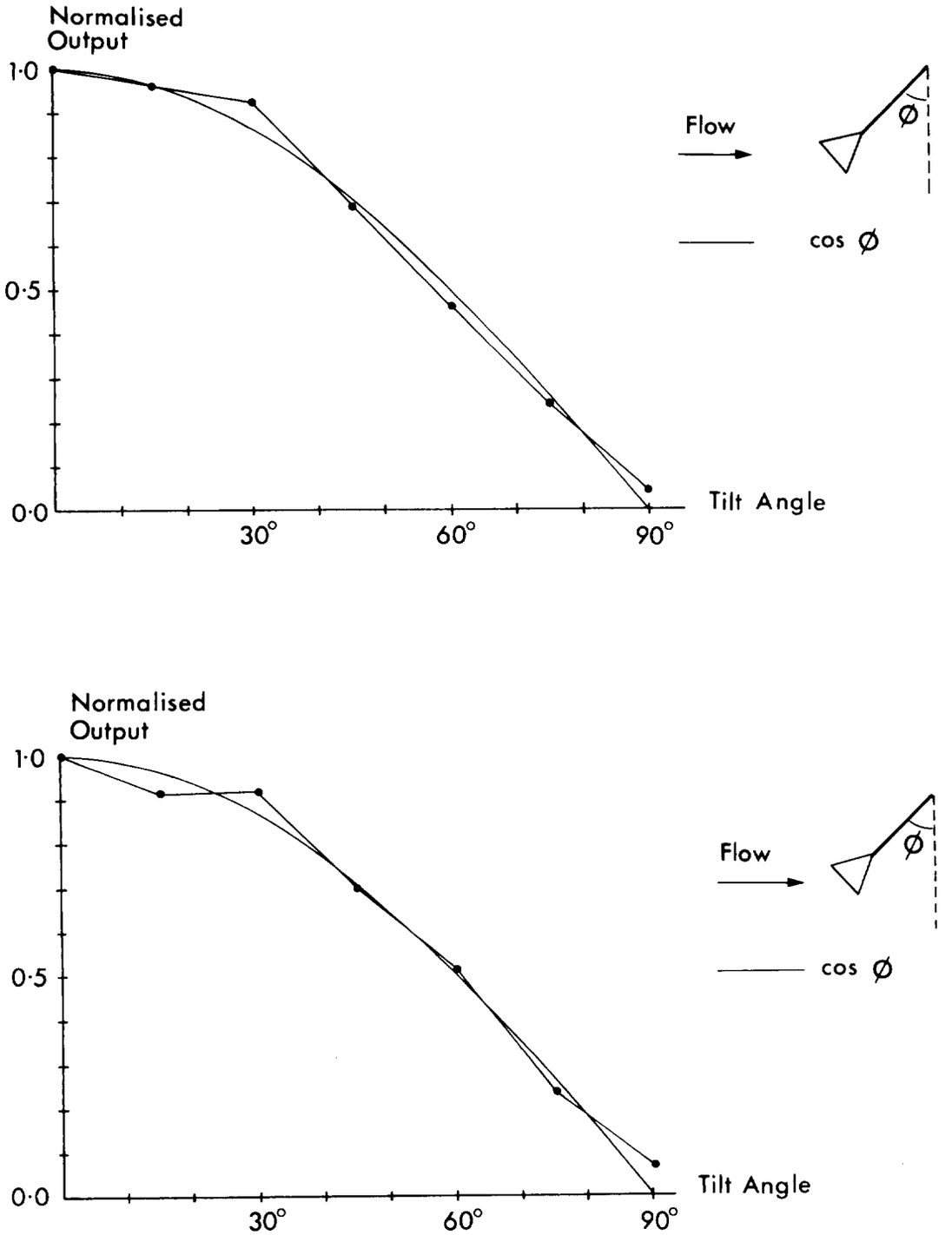

Fig. 17. Response of annular head tilted from vertical mounting at fixed angle ϕ. Azimuth $\phi = 45^{\circ}$.

(a) Speed 12 cm/s. Flow positive.

(b) Speed 60 cm/s. Flow positive.

95% confidence interval is of same order of size as plotted symbol. Uncertainty due to residual flow negligible for (b). Max. of ±0.02 at $\phi = 0$ for (a).

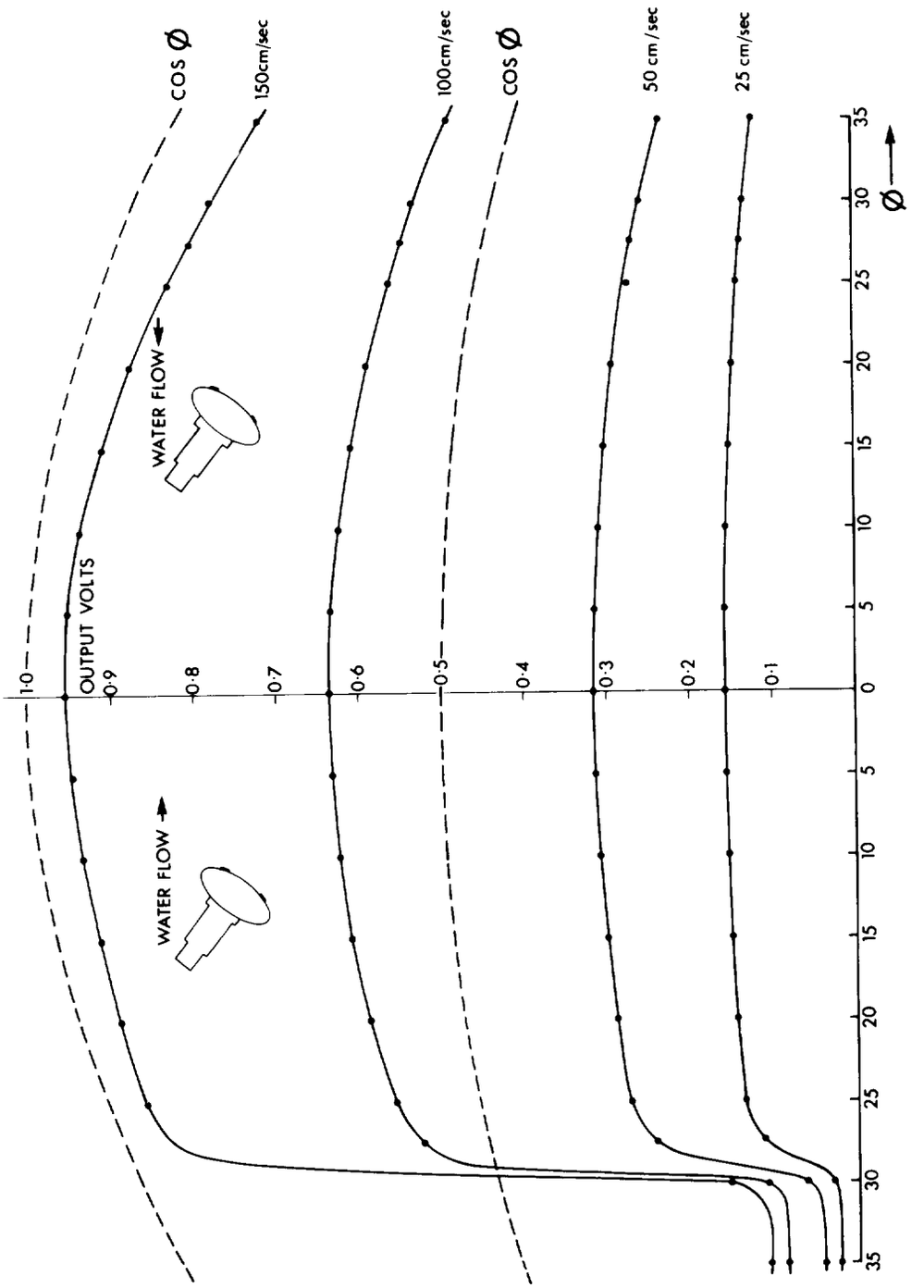

Fig. 18. Response of discus head tilted from vertical mounting (from Tucker, 1972).

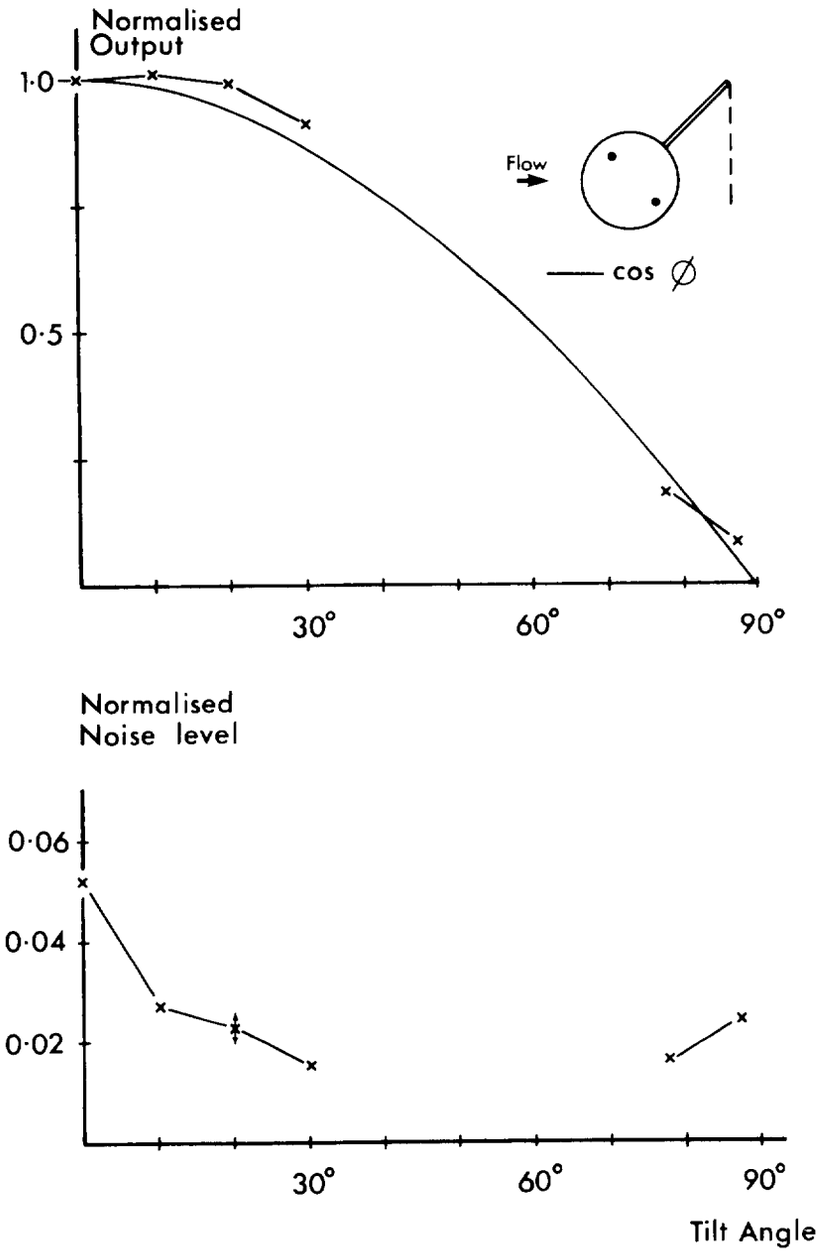

Fig. 19. (a) Response of spherical head (electrode protrusion 1.5 mm) tilted from vertical mounting. Azimuth angle $\theta = 45^{\circ}$. Speed=10 cm s^{-1}.
(b) Noise level expressed as a fraction of output at $\phi = 0^{\circ}$.

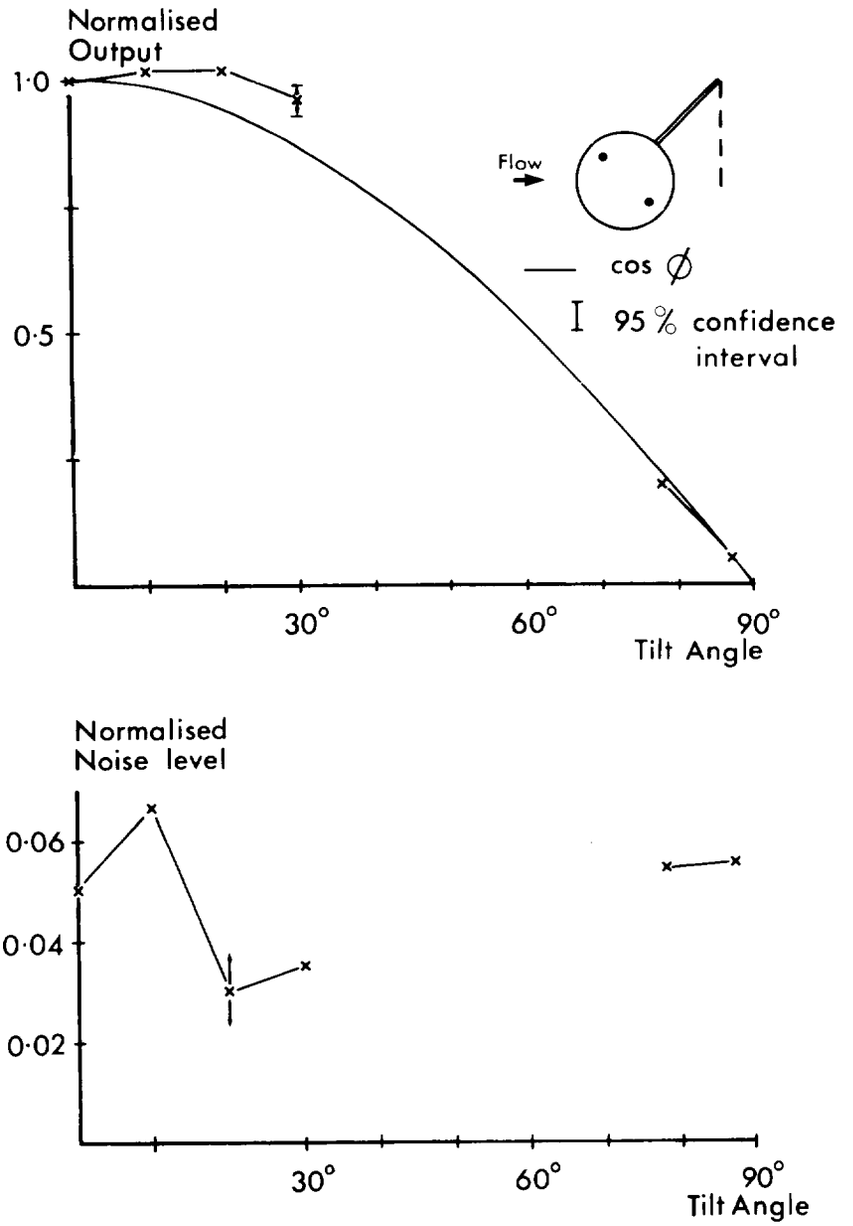

Fig. 20. (a) Response of spherical head (electrode protrusion 1.5 mm) tilted from vertical mounting. Azimuth angle $\theta = 45^{o}$. Speed=47 cm s^{-1}.
(b) Noise level expressed as a fraction of output at $\phi = 0^{o}$.

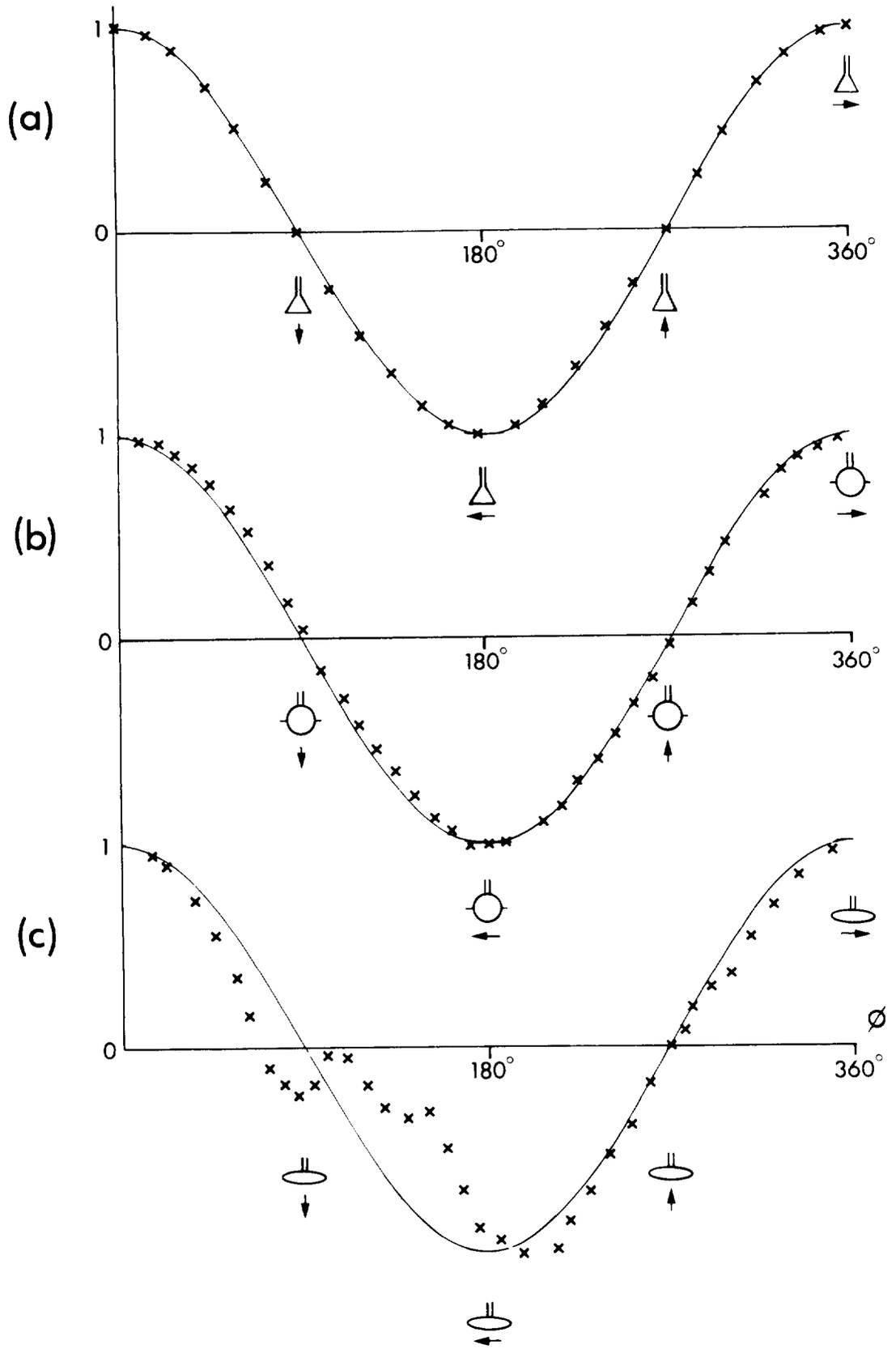

Fig. 21. Dynamic response of three types of sensor head obtained using orbital motion simulator. Azimuth angle = 45°. Arrows denote flow direction.

(a) Annulus. Period 7.5 sec. Orbital dia. 75 cm.

(b) Sphere. Period 7.5 sec. Orbital dia. 75 cm.

(c) Discus. Period 10 sec. Orbital dia. 75 cm.

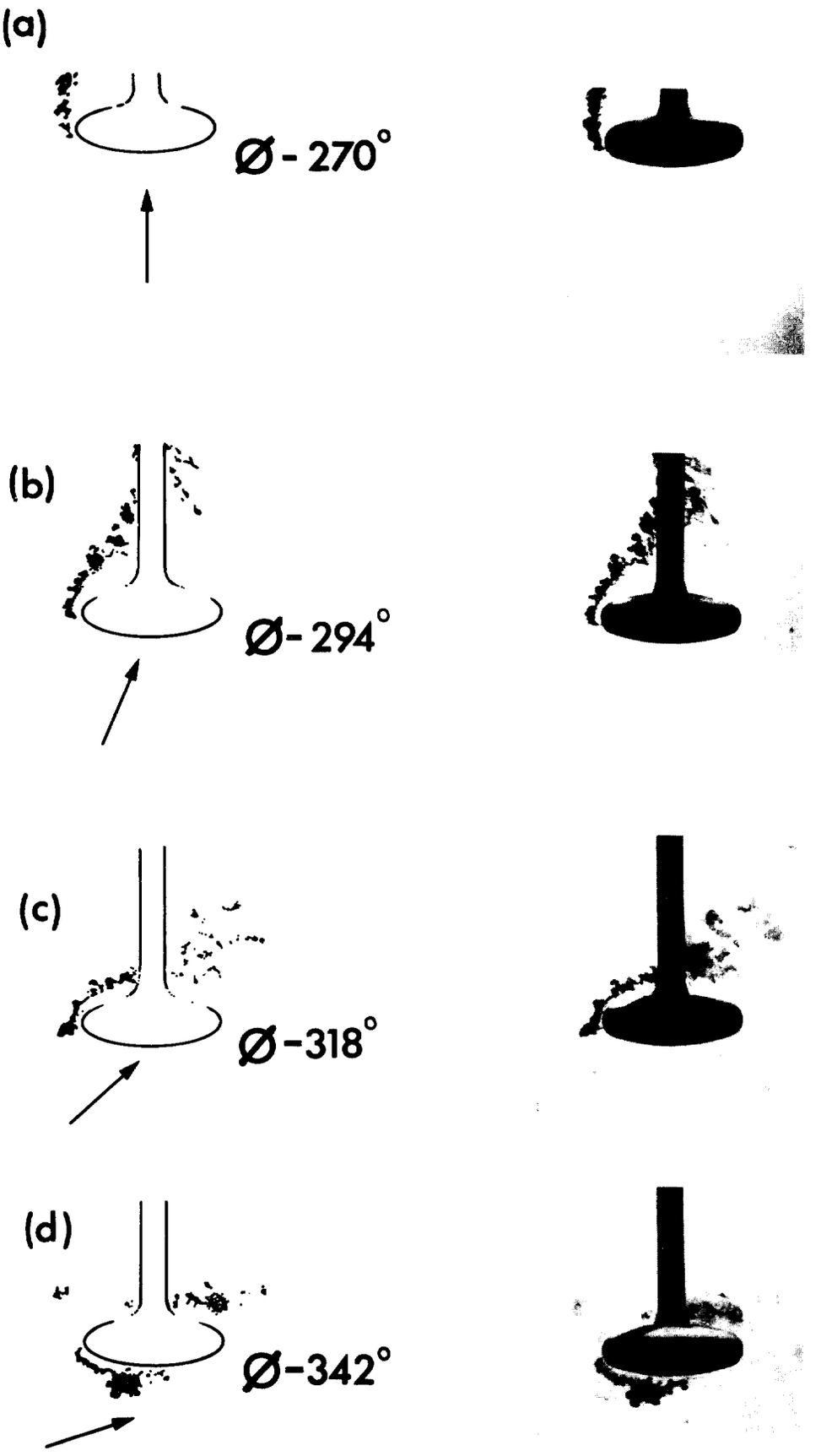

22. Sequence of photographs taken at equal intervals during one revolution of the orbital motion simulator. Potassium permanganate dye ejected from the head shows the stall behaviour in (f)-(i). Angles ϕ correspond with those in fig. 19. Period = 10 sec. Orbital diameter = 0.5 metres. Arrows show flow direction.

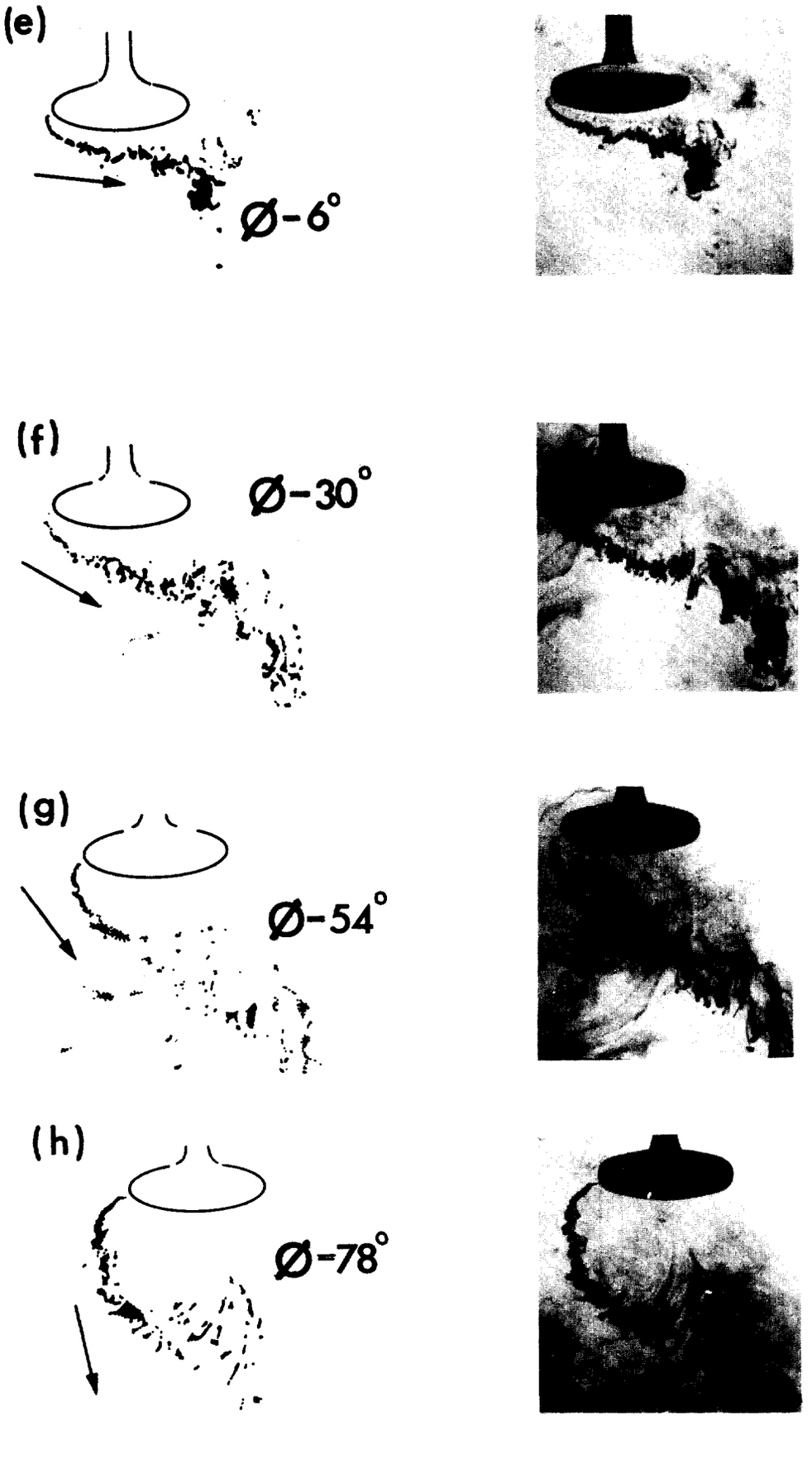
(e)
Ø-6°
(f)
Ø-30°
(g)
Ø-54°
(h)
Ø-78°

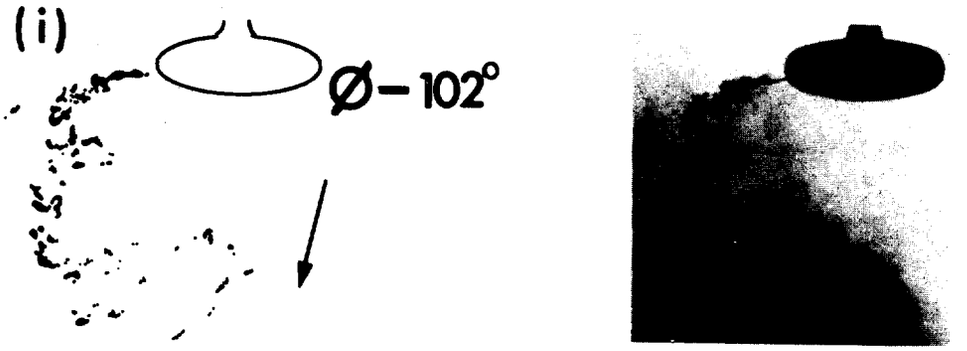
(i)
Ø – 102°

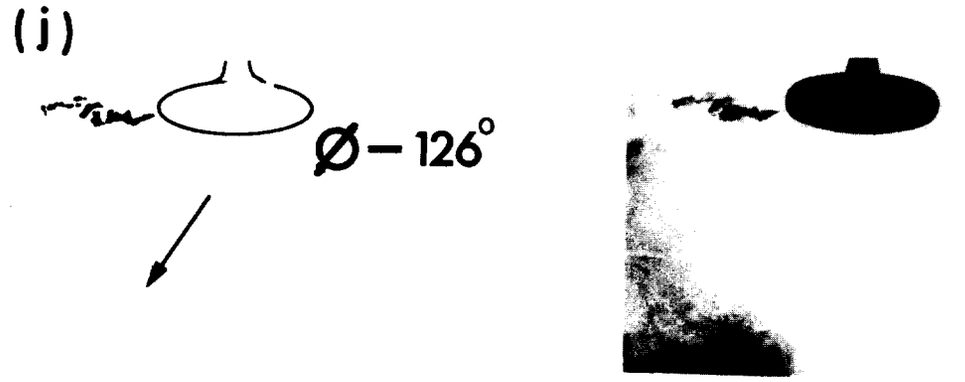
(j)
Ø – 126°


(k)
Ø – 150°

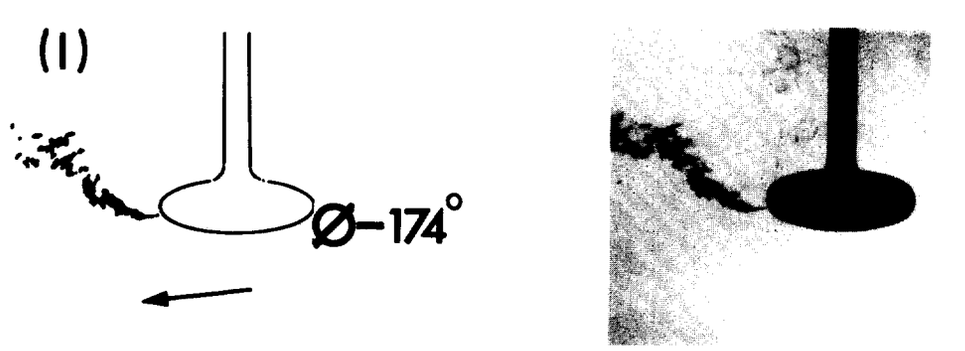
(l)
Ø – 174°

(m)

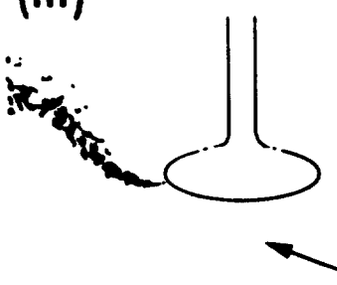

Ø-198°

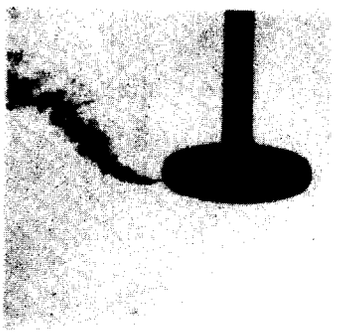

(n)

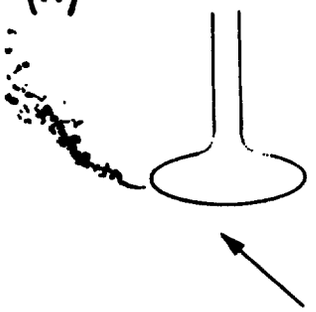

Ø-222°

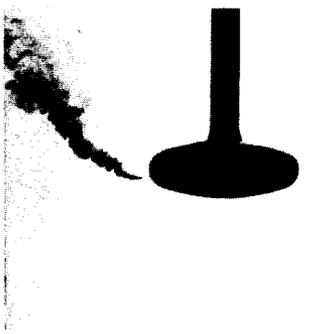

(o)

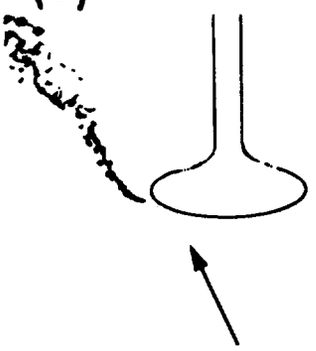

Ø- 246°

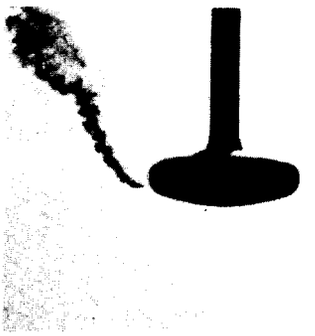

(p)

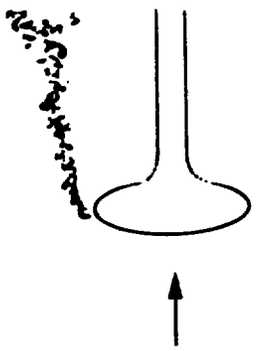

Ø-270°

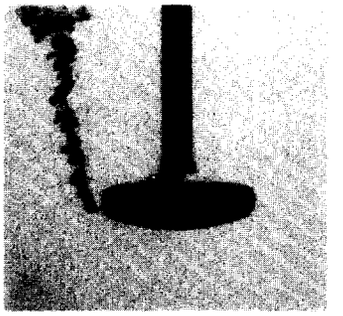

× Orbital motion only. Period 10 sec. Dia. 75 cm.

● Orbital motion (period 2.7 sec, dia. 75 cm; $r\dot{\phi}$ = 90 cm/s).

✚ Translational motion (90 cm/s).

---- Abstracted from Tucker, 1972.

——— Cos ϕ.

Shaded area denotes region of reversed output.

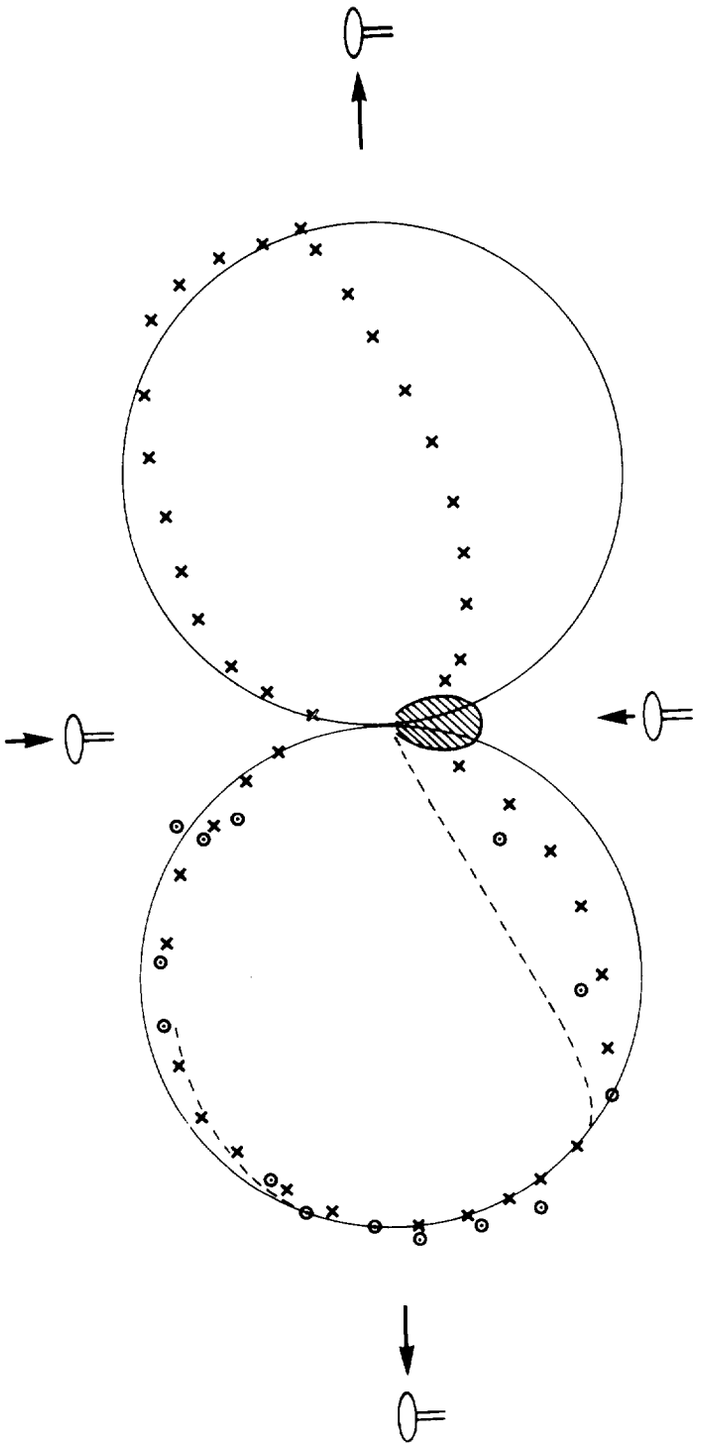

Fig. 23. Dynamic response of discus head in polar form.

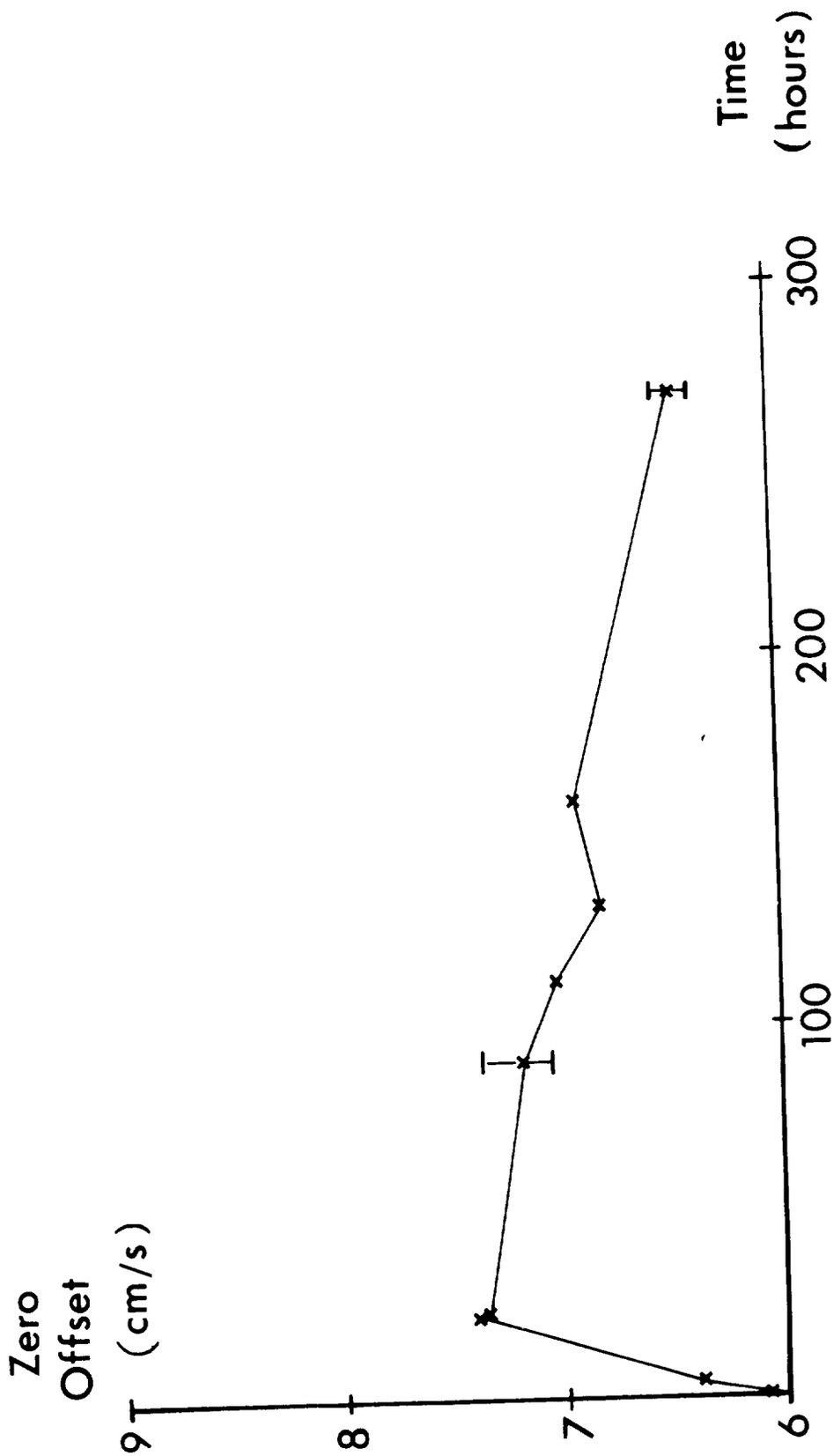

Fig. 24. Variation of zero offset with time for a discus head in fresh water at constant temperature. Error bars denote 95% confidence limits.

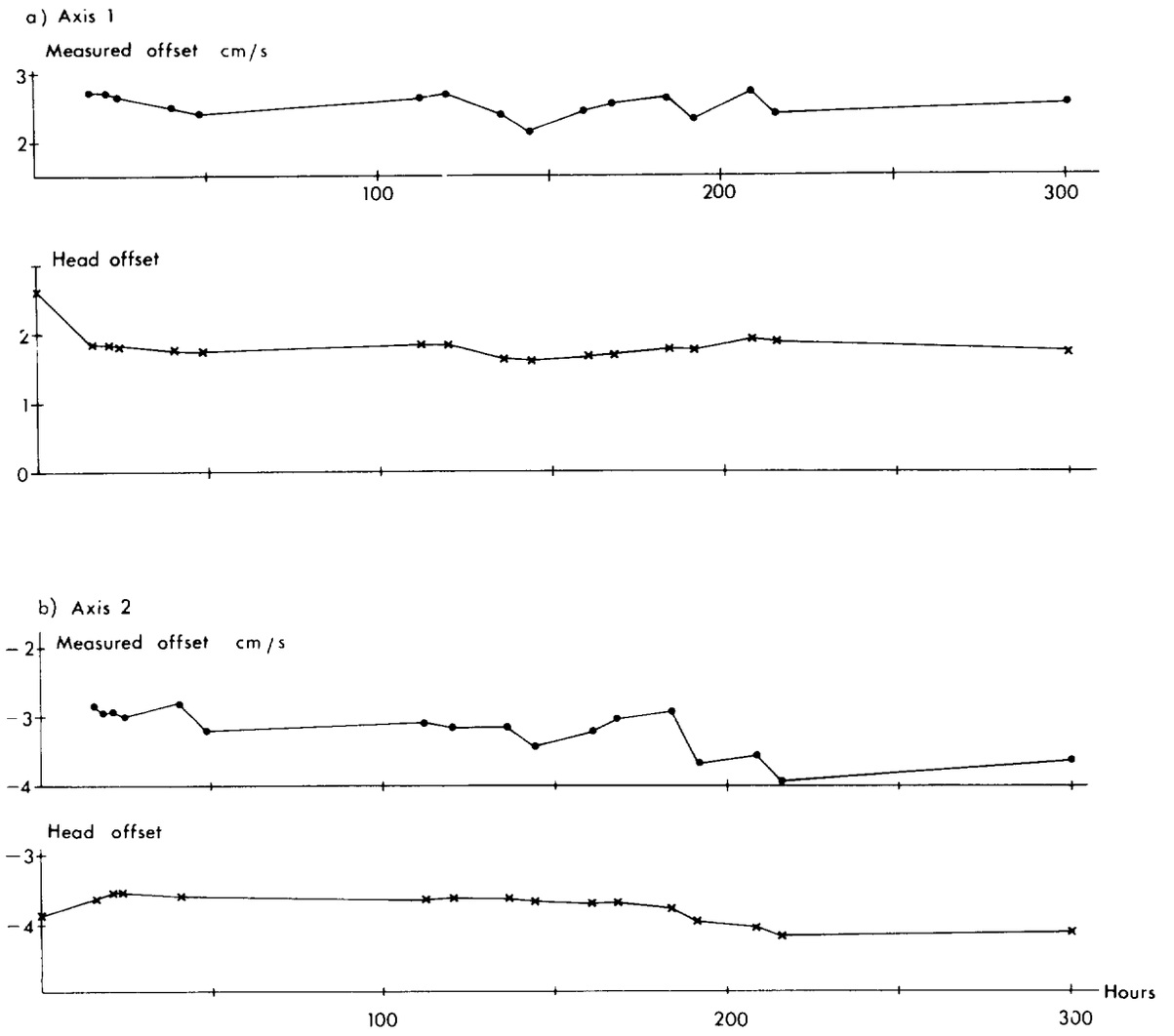

Fig. 25. Variation of measured zero offset with time for early version of annular head in salt water (conductivity 4 Siemens/m). The drift associated with sample and hold, and amplifier circuits was measured by shorting the inputs. This has been subtracted to produce a "head offset" for each axis. 95% confidence limits are of order of plotted symbol size.